



HAL
open science

Dynamic control of the high-affinity iron uptake complex in root epidermal cells

Amanda Martín Barranco, Julien Spielmann, Guillaume Dubeaux, Grégory Vert, Enric Zelazny

► **To cite this version:**

Amanda Martín Barranco, Julien Spielmann, Guillaume Dubeaux, Grégory Vert, Enric Zelazny. Dynamic control of the high-affinity iron uptake complex in root epidermal cells. *Plant Physiology*, 2020, 184 (3), pp.1236-1250. 10.1104/pp.20.00234 . hal-02931857

HAL Id: hal-02931857

<https://hal.science/hal-02931857>

Submitted on 17 Dec 2020

HAL is a multi-disciplinary open access archive for the deposit and dissemination of scientific research documents, whether they are published or not. The documents may come from teaching and research institutions in France or abroad, or from public or private research centers.

L'archive ouverte pluridisciplinaire **HAL**, est destinée au dépôt et à la diffusion de documents scientifiques de niveau recherche, publiés ou non, émanant des établissements d'enseignement et de recherche français ou étrangers, des laboratoires publics ou privés.



Distributed under a Creative Commons Attribution - NonCommercial - NoDerivatives 4.0 International License

1 **Short title:** *Arabidopsis* iron uptake complex

2

3 **Dynamic control of the high-affinity iron uptake complex in root epidermal**
4 **cells**

5

6 Amanda Martín-Barranco¹, Julien Spielmann², Guillaume Dubeaux³, Grégory Vert^{2*}, and
7 Enric Zelazny^{1,4*}

8

9 ¹Institute for Integrative Biology of the Cell (I2BC), UMR9198 CNRS/CEA/Univ. Paris Sud,
10 Université Paris-Saclay, 91198 Gif-sur-Yvette, France.

11 ²Plant Science Research Laboratory (LRSV), UMR5546 CNRS/University of Toulouse 3,
12 31320 Auzeville Tolosane, France.

13 ³Division of Biological Sciences, Cell and Developmental Biology Section, University of
14 California San Diego, La Jolla, CA 92093, USA.

15 ⁴Current address: BPMP, CNRS, INRAE, Montpellier SupAgro, Univ Montpellier, 2 Place
16 Viala, 34060 Montpellier Cedex 2, France.

17

18 *Corresponding authors: Enric.Zelazny@supagro.fr ; Gregory.Vert@lrsv.ups-tlse.fr

19

20

21 The authors responsible for distribution of materials integral to the findings presented in this
22 article in accordance with the policy described in the Instructions for Authors
23 (www.plantphysiol.org) are: Enric Zelazny (Enric.Zelazny@supagro.fr) and Grégory Vert
24 (Gregory.Vert@lrsv.ups-tlse.fr).

25

26 **Author contributions:** A.M.B., G.V. and E.Z. designed the research; A.M.B. J.S. and E.Z.
27 performed the experiments; G.D. performed the quantification of co-localization and
28 statistical analyses; A.M.B., J.S., G.D., G.V. and E.Z. analyzed data; A.M.B., G.V. and E.Z.
29 wrote the manuscript.

30

31 **Funding:** This work has benefited from a French State grant (reference ANR-10-LABX-
32 0040-SPS, to E.Z.) managed by the French National Research Agency under an Investments
33 for the Future program (reference n°ANR-11-IDEX-0003-02). This work was also funded by
34 Marie Curie Actions (PCIG-GA-2012-334021, to G.V.), by the French National Research
35 Agency (ANR-13-JSV2-0004-01, to G.V.) and the French Laboratory of Excellence project
36 “TULIP” (ANR-10-LABX-41 and ANR-11-IDEX-0002-02 to G.V.). Guillaume Dubeaux is
37 supported by an EMBO long-term postdoctoral fellowship (ALTF334-2018).

38

39

40 **One-sentence summary:** The three main actors of iron acquisition in *Arabidopsis* root,
41 namely IRT1, FRO2, and AHA2, assemble into a dedicated protein complex.

42

43

44

45

46

47

48

49

50

51

52

53

54

55

56 **ABSTRACT**

57 In plants, iron uptake from the soil is tightly regulated to ensure optimal growth and
58 development. Iron absorption in *Arabidopsis* root epidermal cells requires the IRT1
59 transporter that also allows the entry of certain non-iron metals, such as Zn, Mn, and Co.
60 Recent work demonstrated that IRT1 endocytosis and degradation are controlled by IRT1
61 non-iron metal substrates in an ubiquitin-dependent manner. To better understand how metal
62 uptake is regulated, we identified IRT1-interacting proteins in *Arabidopsis* roots by mass
63 spectrometry and established an interactome of IRT1. Interestingly, the AHA2 proton pump
64 and the FRO2 reductase, both of which work in concert with IRT1 in the acidification-
65 reduction-transport strategy of iron uptake, were part of this interactome. We confirmed that
66 IRT1, FRO2, and AHA2 associate through co-immunopurification and split-ubiquitin
67 analyses, and uncovered that they form tripartite direct interactions. We characterized the
68 dynamics of the iron uptake complex and showed that FRO2 and AHA2 ubiquitination is
69 independent of the non-iron metal substrates transported by IRT1. In addition, FRO2 and
70 AHA2 are not largely endocytosed in response to non-iron metal excess, unlike IRT1. Indeed,
71 we provide evidence that the phosphorylation of IRT1 in response to high levels of non-iron
72 metals likely triggers dissociation of the complex. Overall, we propose that a dedicated iron-
73 acquisition protein complex exists at the cell surface of *Arabidopsis* root epidermal cells to
74 optimize iron uptake.

75

76 **Keywords:** IRT1, iron, *Arabidopsis*, transport, endocytosis, phosphorylation

77

78

79

80

81

82

83

84

86 **INTRODUCTION**

87 Iron is essential for plant growth and development as it plays fundamental roles in
88 many cellular processes, including photosynthetic and respiratory electron transfer reactions.
89 However, iron is also toxic when present in excess because it induces oxidative stress. Iron
90 bioavailability to plants is often limited, such as in calcareous soils in which iron is present in
91 the form of insoluble complexes (Briat et al., 2015). Iron is a limiting factor for plant biomass
92 production and hence is required as an important component of agriculture productivity. To
93 maintain iron homeostasis, plants must tightly regulate iron absorption from the soil. In non-
94 graminaceous plants, including the model plant *Arabidopsis thaliana*, iron absorption by root
95 epidermal cells is achieved through the so-called strategy I, which requires three successive
96 steps. Firstly, soil ferric chelates are solubilized by local rhizosphere acidification via the
97 release of protons by the proton pump H⁺-ATPase2 (AHA2). Solubilized Fe³⁺ ions are then
98 reduced to Fe²⁺ by the Ferric Reduction Oxydase2 (FRO2) reductase and finally transported
99 into the cell by the iron transporter Iron Regulated Transporter1 (IRT1) (Palmer and Guerinot,
100 2009; Thomine and Vert, 2013; Jeong et al., 2017). During this acidification-reduction-
101 transport mechanism, reduction of Fe³⁺ ions by FRO2 has been proposed to be the rate-
102 limiting step in iron acquisition (Robinson et al., 1999; Connolly et al., 2003). In *Arabidopsis*,
103 the expression of *IRT1*, *FRO2*, and *AHA2* genes is activated under iron-limited conditions
104 through the direct action of the basic Helix-Loop-Helix (bHLH) transcription factor FER-like
105 Iron Deficiency-Induced Transcription Factor (FIT) that can form heterodimers with other
106 bHLH proteins (Colangelo and Guerinot, 2004; Jakoby et al., 2004; Yuan et al., 2008). Apart
107 from the predominant role of IRT1, FRO2, and AHA2, another membrane protein called
108 ATP-Binding Cassette G37 (ABCG37/PDR9) was demonstrated to be involved in
109 *Arabidopsis* iron acquisition by exporting coumarins in the rhizosphere under iron deficiency
110 (Fourcroy et al., 2014). These excreted phenolic compounds chelate Fe³⁺ and facilitate iron
111 availability for reduction by FRO2 (Fourcroy et al., 2016). Similar to the other components of
112 the *Arabidopsis* iron-acquisition machinery, the *ABCG37/PDR9* gene is transcriptionally
113 induced in response to iron deficiency in a FIT-dependent manner (Rodriguez-Celma et al.,
114 2013).

115 IRT1 is a major player in the regulation of plant iron homeostasis, as attested by the
116 severe chlorosis and the lethality of the *irt1-1* knock-out mutant (Vert et al., 2002).
117 Interestingly IRT1 is a broad-spectrum transporter, which also allows the absorption of metals

118 such as zinc, manganese, cobalt, and cadmium, in addition to iron (Rogers et al., 2000; Vert et
119 al., 2001; Vert et al., 2002). The dynamics of IRT1 protein and its role in the maintenance of
120 metal homeostasis in *Arabidopsis* have been widely investigated. IRT1 localizes to early
121 endosomes in root epidermal cells and rapidly cycles between this compartment and the cell
122 surface to perform iron absorption (Barberon et al., 2011). Importantly, IRT1 dynamics
123 requires clathrin-mediated endocytosis and is controlled by ubiquitination on two cytosol-
124 exposed lysine residues (Barberon et al., 2011), a process mediated by the E3 ubiquitin ligase
125 IRT1 DEGRADATION FACTOR1 (IDF1) (Shin et al., 2013; Dubeaux et al., 2018).
126 Surprisingly, IRT1 ubiquitination and endocytosis are not regulated by iron, the primary
127 substrate of the IRT1 transporter, but rather by its secondary metal substrates (Zn, Mn, and
128 Co, herein called non-iron metal substrates). These non-iron metal substrates, which are
129 highly reactive and toxic when present in excess in plant cells, were recently demonstrated to
130 regulate IRT1 endocytosis (Barberon et al., 2014). In the presence of physiologically relevant
131 concentrations of non-iron metal substrates, a functional IRT1-mCitrine fusion protein is
132 localized in early endosomes and to some extent at the plasma membrane of root epidermal
133 cells. Interestingly, in the presence of an excess of non-iron metal substrates, IRT1-mCitrine
134 is targeted to late endosomes and then reaches the vacuole for degradation, whereas it is
135 exclusively localized to the plasma membrane in the absence of such metals. The sensing of
136 the excess of non-iron metal substrates is directly mediated by IRT1 through the binding of
137 metals on a histidine-rich stretch located in IRT1 large cytosolic loop (Dubeaux et al., 2018).
138 Hence, IRT1 was proposed to act as a transceptor, combining transporter and receptor
139 properties (Cointry and Vert, 2019). Non-iron metal binding to IRT1 allows the recruitment
140 of Calcineurin B-like (CBL)-interacting serine/threonine-protein kinase 23 (CIPK23) and
141 subsequent phosphorylation of IRT1. This in turn allows the lysine-63 polyubiquitination of
142 IRT1 by IDF1, triggering IRT1 endocytosis and targeting to the vacuole (Dubeaux et al.,
143 2018). The control of IRT1 degradation by its secondary substrates certainly constitutes a
144 protective mechanism allowing limitation of the absorption of readily available Zn^{2+} , Mn^{2+} ,
145 and Co^{2+} ions that, contrary to Fe^{3+} , do not need prior reduction by FRO2 to be transported
146 (Zelazny et al., 2011). Interestingly, the plasma membrane pool of IRT1 is present at the outer
147 polar domain of root epidermal cells, which is necessary for proper radial transport of metals
148 in the root (Barberon et al., 2014). IRT1 physically interacts with FYVE1, a protein recruited
149 to the Endosomal Sorting Complexes Required for Transport (ESCRT) in late endosomes
150 (Barberon et al., 2014; Gao et al., 2014). FYVE1 drives the maintenance of IRT1 lateral
151 polarity, through a mechanism that is not fully understood. Interference with *FYVE1*

152 expression induces apolar localization of IRT1 at the plasma membrane and disturbs metal
153 uptake in *Arabidopsis* (Barberon et al., 2014). IRT1 recycling from endosomes to the plasma
154 membrane was shown to require Sorting Nexin 1 (SNX1) (Ivanov et al., 2014). Recently, the
155 peripheral membrane protein ENHANCED BENDING1 (EHB1) was demonstrated to interact
156 with IRT1 in a calcium-dependent manner and was proposed to act as an inhibitor of IRT1-
157 mediated iron transport (Khan et al., 2019).

158 Since IRT1 is an essential determinant of root metal uptake in low-iron conditions, we
159 sought to identify additional proteins involved in IRT1 dynamics/activity or working in
160 concert with IRT1 to better characterize how plant metal homeostasis is controlled. Using co-
161 immunopurification (co-IP) of IRT1 and identification of IRT1-interacting proteins by mass
162 spectrometry, we shed light on the existence of a dedicated protein complex composed of
163 IRT1, FRO2, and AHA2 that likely optimizes iron uptake in root epidermal cells. We also
164 uncovered that IRT1 is selectively removed from the complex in response to non-iron metal
165 excess, in a process involving its phosphorylation.

166

167 **RESULTS**

168 **IRT1 interactome in *Arabidopsis* root epidermal cells**

169 To better understand how the non-iron metal-mediated internalization of IRT1 is
170 controlled in root epidermal cells, we searched for proteins interacting with IRT1 upon non-
171 iron metal excess. To this purpose, a functional IRT1-mCitrine fusion protein expressed under
172 the control of the *IRT1* promoter in *Arabidopsis irt1-1* null mutant (Dubeaux et al., 2018) was
173 immunopurified, and co-purified proteins were identified by mass spectrometry. *irt1-1*/
174 *IRT1::IRT1-mCitrine* transgenic line and *Ws* wild-type (WT) plants, used as a negative
175 control, were initially grown for nine days on MS/2 medium containing iron, transferred for
176 five days onto a medium lacking iron and containing physiological concentrations of non-iron
177 metals to induce IRT1-mCitrine expression, and finally transferred to a medium without iron
178 and containing an excess of non-iron metal substrate for two days. To purify the
179 transmembrane IRT1-mCitrine protein, root protein extracts from IRT1-mCitrine-expressing
180 plants were solubilized with a soft non-ionic detergent, n-Dodecyl β -D-maltoside (DDM), to
181 preserve the interactions between IRT1 and its partners. Then, IRT1-mCitrine and the
182 associated proteins were immunopurified with anti-GFP antibodies coupled to magnetic
183 microbeads, the same procedure was performed on DDM-solubilized proteins from WT plant

184 roots. Immunopurified proteins from IRT1-mCitrine and WT plants were separated by SDS-
185 PAGE (Supplemental Fig. 1) and analyzed by mass spectrometry. Proteins were considered as
186 interacting with IRT1 when specifically identified in IRT1-mCitrine immunopurified fraction
187 with at least two different peptides. This approach allowed the identification of 142 putative
188 IRT1 interactants (Supplemental Dataset 1). Among these, 31 were found in the two
189 independent experiments whereas 111 were detected in only one of the two replicates. Since
190 the control of IRT1 trafficking is of the utmost importance for the regulation of this
191 transporter, we specifically looked for IRT1-interacting proteins that are linked to the
192 secretory or endocytic pathways (Table1). Clathrin was found as putatively interacting with
193 IRT1, which is in accordance with our previous results showing that IRT1 undergoes clathrin-
194 mediated endocytosis (Barberon et al., 2011; Barberon et al., 2014). Interestingly SEC13a and
195 SEC31b proteins were identified as IRT1 putative interactants, suggesting a role of coat
196 protein complex II (COPII) machinery in the export of IRT1 from the endoplasmic reticulum
197 (ER) to the Golgi apparatus (Chung et al., 2016). Conversely, IRT1 probably also undergoes
198 retrograde transport from the Golgi to the ER since it interacts with components of COPI
199 vesicles (Table 1) (Yorimitsu et al., 2014). Another interesting group of IRT1 interactants are
200 proteins linked to *Arabidopsis* metal homeostasis such as the Pleiotropic drug resistance 8 /
201 Penetration 3 protein that was proposed to act as a cadmium extrusion pump (Kim et al.,
202 2007) (Table 1). IRT1 also associates with two iron transporters from the VIT family;
203 however, the relevance of this interaction remains unclear since these proteins were described
204 as localizing to the ER body membrane (Yamada et al., 2013). Recently, rhizosphere-excreted
205 coumarins were shown to be important for iron acquisition in an IRT1-dependent manner
206 (Fourcroy et al., 2016). Interestingly, the Feruloyl-Coenzyme A 6'-Hydroxylase 1 (F6'H1)
207 (Schmid et al., 2014) and the Cytochrome P450/CYP82C4 (Rajniak et al., 2018), which are
208 both involved in coumarin biosynthesis, were identified as putative IRT1-interacting proteins
209 (Table 1). In addition, FRO2 and AHA2, which are known to both act in concert with IRT1 in
210 the acidification-reduction-transport strategy for iron uptake in *Arabidopsis thaliana*, were
211 also identified (Table 1). Mass spectrometry analyses performed on IRT1 co-immunopurified
212 fractions indeed identified peptides specific to the AHA2 isoform, but also identified peptides
213 common to AHA2 and other AHA proteins, mostly AHA1. However, since no peptide
214 specific to other AHA proteins than AHA2 were found, and because rhizosphere acidification
215 is chiefly mediated by AHA2 in lack of iron (Santi and Schmidt, 2009), we decided to focus
216 our attention on AHA2. These observations indicate that IRT1, FRO2, and AHA2 likely
217 associate to drive iron uptake. To gain further insight into the regulation of the iron uptake

218 machinery, we characterized in more detail the interaction and the spatial organization of the
219 three major actors of iron acquisition, namely FRO2, AHA2, and IRT1.

220

221 **IRT1 directly interacts with FRO2 and AHA2**

222 To validate the observations obtained from mass spectrometry analyses, the
223 interactions between IRT1 and AHA2/FRO2 were first investigated in *Arabidopsis* roots by
224 performing co-IP combined with immunodetections. We analyzed the interaction between
225 IRT1-mCitrine, expressed under the control of *IRT1* promoter, and endogenous AHA2 protein
226 by using a previously described antibody raised against Plasma Membrane H⁺-ATPase 2
227 (PMA2) from *Nicotiana plumbaginifolia* that recognizes AHA2 and also other *Arabidopsis*
228 AHA proteins. When IRT1-mCitrine IP fraction was probed with anti-PMA2 antibodies, a
229 strong signal corresponding to the expected size of AHA2 (104 kDa) was detected, whereas
230 no signal was observed in the IP fraction from WT plant roots used as a negative control (Fig.
231 1A). Although this signal may correspond in part to other AHA isoforms than AHA2 due to a
232 lack of specificity of the anti-PMA2 antibodies, this result suggests that endogenous AHA2
233 likely associates with IRT1 in root epidermal cells. The existence of an IRT1-AHA2 complex
234 is substantiated by other protein-protein interaction assays described hereafter. Since no
235 antibody raised against FRO2 was available, we generated a translational fusion of FRO2
236 expressed under control of the *FRO2* promoter in the previously described *fro2* mutant named
237 *frd1-1* (Robinson et al., 1999). Expression of FRO2 fused at its N-terminal end to the
238 mCherry fluorescent protein (mCherry-FRO2) complemented the hypersensitivity of *frd1-1* to
239 low iron, even for transgenic lines expressing low levels of mCherry-FRO2 (Supplemental
240 Fig. 2A and B). This clearly shows that mCherry-FRO2 fusion protein is fully functional.
241 Consistently, mCherry-FRO2 protein was only detected in root epidermal cells (Supplemental
242 Fig. 2C), highlighting the specificity of *FRO2* promoter, as previously reported (Connolly et
243 al., 2003). To analyze the interaction between FRO2 and IRT1 in *Arabidopsis* roots by co-IP,
244 we generated transgenic lines co-expressing mCherry-FRO2 and IRT1-mCitrine under control
245 of the *FRO2* and *IRT1* promoters, respectively. Transgenic lines co-expressing IRT1-mCitrine
246 and RabD1-mCherry, the latter co-localizing with IRT1 in endosomes (Supplemental Fig. 3),
247 were used as a negative control. mCherry-FRO2 was co-immunopurified with IRT1-mCitrine
248 whereas RABD1-mCherry was not, proving that FRO2 and IRT1 form a protein complex in
249 root epidermal cells (Fig. 1B and Supplemental Fig. 4).

250 The interaction between IRT1 and AHA2/FRO2 was also confirmed by a split-
251 ubiquitin assay, which allows the detection of direct interactions between membrane proteins
252 in yeast. Such an approach has been successfully implemented with IRT1 and IDF1 (Shin et
253 al., 2013; Dubeaux et al., 2018). IRT1 fused to the mutated N-terminal half of ubiquitin
254 (NubG), which is unable to spontaneously reassemble with the C-terminal part of ubiquitin
255 (Cub), was co-expressed in yeast with AHA2 or FRO2 fused to Cub linked to the chimeric
256 transcription factor ProteinA-LexA-VP16 (PLV) (Fig. 1C). Physical interactions between
257 IRT1 and AHA2/FRO2 were tested through the ability to rescue yeast growth on a selective
258 medium. Yeast co-expressing NubG-IRT1 with AHA2-Cub or FRO2-Cub grew on a selective
259 medium, similarly to the respective positive controls expressing NubWT with AHA2-
260 Cub/FRO2-Cub. However, no growth was observed for the respective negative controls
261 expressing NubG with AHA2-Cub/FRO2-Cub. As an additional negative control for split-
262 ubiquitin, NubG-IRT1 was co-expressed with an unrelated transmembrane protein,
263 specifically the brassinosteroid receptor BRI1, fused to Cub. Whereas yeast co-expressing
264 NubWT with BRI1-Cub (positive control of interaction) grew on a selective medium, no
265 growth was observed when BRI1 and IRT1 were co-expressed, indicating that these two
266 proteins do not interact. Interestingly, our split-ubiquitin assay also revealed that AHA2 and
267 FRO2 could physically associate with each other (Fig. 1C). This result was confirmed in
268 plants by co-IP approaches showing that endogenous AHA2 is co-immunopurified with
269 mCherry-FRO2 from *Arabidopsis* root protein extracts (Supplemental Fig. 5). Altogether,
270 these observations validate the existence of a protein complex in root epidermal cells that
271 gathers the different actors of the high-affinity iron uptake machinery in close proximity.

272

273 **Differential regulation of the iron uptake system by ubiquitination**

274 We recently demonstrated that IRT1 endocytosis is controlled by the non-iron metal
275 substrates of IRT1 (Dubeaux et al., 2018). Upon an excess of these metals, IRT1
276 ubiquitination strongly increases leading to the endocytosis and the degradation of IRT1 in
277 the vacuole. Interestingly, proteomic analyses allowed the identification of AHA2 and FRO2
278 as part of the *Arabidopsis* ubiquitinome (Kim et al., 2013; Johnson and Vert, 2016; Walton et
279 al., 2016). Since AHA2 and FRO2 belong to an IRT1-containing protein complex, we
280 wondered whether ubiquitination of these proteins could be co-regulated by non-iron metal
281 availability. First, we analyzed the ubiquitination profile of AHA2 and FRO2 by performing

282 IP of AHA2-GFP and mCherry-FRO2 expressed in *Arabidopsis* roots, followed by the
283 immunodetection of ubiquitination with the P4D1 general anti-ubiquitin antibodies. In the
284 presence of physiological concentrations of non-iron metal substrates, AHA2-GFP and
285 mCherry-FRO2 IP fractions probed with P4D1 antibodies exhibited high-molecular-weight
286 smears that are typical of ubiquitinated proteins as observed for IRT1-mCitrine used as a
287 control (Fig. 2). To quantify the effect of non-iron metal regime on the ubiquitination of the
288 investigated proteins, the signal intensity observed for the anti-ubiquitin immunoblots
289 performed on IRT1-mCitrine, AHA2-GFP, or mCherry-FRO2 immunopurified proteins was
290 measured and normalized to the corresponding immunopurified proteins (Fig. 2C). As
291 previously observed (Dubeaux et al., 2018), a short treatment with an excess of non-iron
292 metals led to a strong increase in IRT1-mCitrine ubiquitination (Fig. 2A and C). By contrast,
293 the pool of ubiquitinated AHA2-GFP and mCherry-FRO2 remained unchanged in both metal
294 regimes (Fig. 2A, B and C, and Supplemental Fig. 6). Hence, although AHA2, FRO2, and
295 IRT1 belong to the same complex involved in a common mechanism i.e. iron acquisition,
296 ubiquitination of these proteins is differentially regulated by metal availability.

297

298 **Selective endocytosis of IRT1 in response to non-iron metal excess**

299 Although the intracellular dynamics of IRT1 and AHA2 were previously
300 independently investigated (Barberon et al., 2011; Dubeaux et al., 2018; Haruta et al., 2018),
301 the subcellular distribution of FRO2 has not previously been determined. Thus, the respective
302 localization of IRT1-mCitrine and FRO2/AHA2 expressed as mCherry fusion proteins was
303 investigated. We used root-tip epidermal cells as i) these cells are well suited to analyze the
304 precise localization of endocytosed plasma membrane proteins and ii) the metal-triggered
305 endocytosis of IRT1 was already characterized in such cells (Dubeaux et al., 2018).
306 Interestingly, in the absence of iron and in the presence of physiologically relevant amounts
307 of non-iron metal substrates, mCherry-FRO2 was present at the plasma membrane in the outer
308 polar domain facing the rhizosphere, as observed for IRT1-mCitrine (Fig. 3A, left panel)
309 (Barberon et al., 2014; Dubeaux et al., 2018). FRO2 also co-localized with IRT1 in
310 intracellular vesicles (Mander's coefficient, $M2 = 0.48$) (Fig. 3A, left panel and 3C), which
311 correspond to early endosomes since IRT1 constitutes a marker of these compartments in
312 such metal conditions (Barberon et al., 2011; Dubeaux et al., 2018). In contrast to IRT1 and
313 FRO2, AHA2-mCherry displayed an apolar plasma membrane localization in epidermal cells

314 in the same metal conditions and although AHA2-mCherry was observed in a limited number
315 of endosomes, these were mostly co-labeled with IRT1-mCitrine ($M2 = 0.39$) (Fig. 3B, left
316 panel and 3D).

317 The intracellular dynamics of FRO2 and AHA2 were then investigated after a short-
318 term treatment with an excess of non-iron metal substrates that triggers IRT1 endocytosis and
319 its subsequent degradation (Dubeaux et al., 2018). Upon non-iron metal excess, IRT1-
320 mCitrine was depleted from the cell surface and accumulated in late endosomes (Fig. 3A and
321 3B, left panels). mCherry-FRO2 and AHA2-mCherry were, however, mostly detected at the
322 plasma membrane, even though they were also found to co-localize with IRT1-mCitrine in
323 late endosomes (Fig. 3A and 3B, left panels). To quantify the response to metals, the ratio of
324 plasma membrane to intracellular fluorescence signal intensities was measured for the three
325 fusion proteins under physiological non-iron metal provision or in the presence of an excess
326 of these metals (Fig. 3A and 3B, right panels). As previously reported, the plasma
327 membrane/intracellular ratio highly decreased for IRT1-mCitrine in response to non-iron
328 metal excess (Dubeaux et al., 2018). For mCherry-FRO2 and AHA2-mCherry, however, no
329 significant difference was observed, indicating that FRO2 and AHA2 are not largely
330 endocytosed in response to non-iron metal excess. However, the level of co-localization of
331 FRO2 and IRT1 in endosomes significantly increased with non-iron metal excess ($M2 = 0.69$)
332 compared to control conditions ($M2 = 0.48$) (Fig. 3C), suggesting a minor effect of non-iron
333 metal status on FRO2 endocytosis. On the other hand, the co-localization level between
334 AHA2 and IRT1 in endosomes was not significantly modified by non-iron metal substrates
335 (Fig. 3D).

336 The absence of a massive internalization of FRO2 and AHA2 in response to non-iron
337 metal excess suggests that the IRT1/FRO2/AHA2 complex dissociates prior to IRT1
338 endocytosis. Since the phosphorylation of residues in the large cytosolic loop of IRT1 was
339 shown to be the trigger of IRT1 ubiquitin-dependent endocytosis upon non-iron metal
340 substrate excess (Dubeaux et al., 2018), we investigated whether phosphomimic (IRT1_{S/TxD})
341 or non-phosphorylatable (IRT1_{S/TxA}) variants of IRT1 would display modified association
342 with AHA2 and FRO2. Using split-ubiquitin approaches, we observed that yeast co-
343 expressing NubG-IRT1_{S/TxD} and AHA2- or FRO2-Cub grew slower on the selective medium
344 than yeast co-expressing NubG-IRT1 or NubG-IRT1_{S/TxA} together with AHA2- or FRO2-Cub
345 (Fig. 4A, B). To better quantify the effect of the respective IRT1 variants, we measured yeast
346 growth in liquid cultures. We consistently observed reduced growth for yeast co-expressing

347 FRO2 or AHA2 with IRT1_{S/TxD} compared to their wild-type or IRT1_{S/TxA} counterparts (Fig.
348 4C, D), although NubG-IRT1_{S/TxD} protein accumulated to the same extent as wild-type or
349 IRT1_{S/TxA} when expressed in yeast cells (Supplemental Fig. 7). These results show that the
350 phosphomimic variant of IRT1 displays a reduced interaction with AHA2 and FRO2.
351 Altogether, these observations clearly indicate a role for IRT1 phosphorylation in dissociation
352 of the high-affinity iron uptake complex upon non-iron metal excess.

353 **DISCUSSION**

354 **IRT1 interactome: new insight into IRT1 dynamics and metal uptake**

355 IRT1 mediates the absorption of iron but also non-iron metal substrates such as Zn,
356 Mn, and Co in root epidermal cells and is a major actor of metal nutrition in *Arabidopsis*.
357 Previous studies revealed that the tight control of IRT1 intracellular dynamics by IDF1,
358 CIPK23, FYVE1, or SNX1 is essential to maintain metal homeostasis and to ensure optimal
359 plant growth and development (Shin et al., 2013; Barberon et al., 2014; Ivanov et al., 2014;
360 Dubeaux et al., 2018). To better understand how IRT1 is controlled in the cell, we searched
361 for further IRT1-interacting proteins by performing IP of the functional IRT1-mCitrine fusion
362 protein expressed under the control of *IRT1* promoter coupled to mass spectrometry analyses.
363 Co-IP has the great advantage to reveal physiologically relevant protein-protein interactions
364 in plant cells and regarding false positives, co-IP does not generate more than the yeast two-
365 hybrid or the split-ubiquitin techniques and results in less than using bimolecular fluorescence
366 complementation (BiFC) (Xing et al., 2016). Besides, co-IP was successfully used in the past
367 to identify interactants of channels and receptors (Karlova et al., 2006; Bellati et al., 2016).
368 One must consider that an interactome provides an overview of proteins putatively interacting
369 with a bait, but that each candidate protein has to be validated by an independent protein-
370 protein interaction technic before further investigation to avoid putative artifacts. Here, we
371 decided to (i) use the *IRT1* endogenous promoter to maximize the detection of interactions
372 between IRT1 and its interactants in relevant cell types, i.e. root epidermal cells, and (ii)
373 validate each candidate of interest using the split-ubiquitin technic. Two independent co-
374 IP/mass spectrometry experiments were performed, which provides qualitative data on
375 proteins interacting with IRT1. Using another replicate would have certainly allowed us to
376 obtain more quantitative data. Besides, since several very interesting candidates such as FRO2
377 were identified in one of the two experiments, we decided to include the proteins that were
378 identified in only one replicate in the IRT1 interactome. Among 142 proteins putatively

379 interacting with IRT1, a group of proteins related to intracellular trafficking emerged, which
380 included clathrin, tubulin, and actin (Table 1). An association between clathrin and IRT1 is in
381 agreement with the previously reported clathrin-mediated internalization of IRT1 from the
382 plasma membrane (Barberon et al., 2014). The co-IP approach does not allow the
383 determination of whether two proteins directly interact or not; however, according to what is
384 known for other cargo proteins, it is likely that the interaction between IRT1 and clathrin is
385 mediated by an unknown adaptor protein. So far the role of actin and tubulin in IRT1
386 dynamics is poorly understood; however, since these proteins are known to be involved in
387 plant endocytosis (Fan et al., 2015), their presence in the IRT1-interactome also opens
388 interesting perspectives. Two small G proteins from the Rab class, namely RAB GTPase
389 homolog A1D and RAB GTPase homolog 1C, were also identified as putative interactants of
390 IRT1 (Table 1). Although the role of these two proteins in intracellular trafficking is still
391 elusive, similar Rab proteins were described to act in plant endocytic pathways (Qi and
392 Zheng, 2013). Intriguingly, the IDF1 E3 ubiquitin ligase and the CIPK23 kinase that are
393 important for IRT1 endocytosis and were demonstrated to interact with IRT1 in split-ubiquitin
394 and yeast-two hybrid candidate approaches, respectively (Shin et al., 2013; Dubeaux et al.,
395 2018), were not co-purified with IRT1 in the present study. Given the functions of IDF1 and
396 CIPK23, their interactions with IRT1 are probably very transient and may be lost during the
397 co-IP procedure contrary to other systems such as split-ubiquitin and yeast-two hybrid where
398 these associations would be stabilized (Xing et al., 2016). Until now, studies of IRT1
399 trafficking in plant cells mainly described endocytic mechanisms including IRT1
400 internalization from the plasma membrane in an ubiquitin-dependent process or IRT1
401 recycling from endosomes to the plasma membrane. How IRT1 traffics along the secretory
402 pathway to reach the plasma membrane remains largely unknown, even though *Malus*
403 *xiaojinesis* IRT1 was proposed to exit the ER in COPII vesicles (Tan et al., 2018). The
404 *Arabidopsis* IRT1 interactome provides interesting clues on these aspects since IRT1 was
405 found to putatively interact with several components of the COPII machinery that is
406 sequentially recruited to the surface of the ER membrane to induce the formation of transport
407 vesicles and ensure the delivery of cargo proteins to the Golgi apparatus (Chung et al., 2016)
408 (Table 1). Membrane proteins exit the ER via the recognition of specific cytoplasmic export
409 motifs by the COPII machinery; these signals include diacidic motifs corresponding to
410 (D/E)_x(D/E), with x representing any amino acid residue (Zelazny et al., 2009). A diacidic
411 motif (EDD) located in the large cytosolic loop of IRT1 at the position 180 may be involved

412 in the packaging of IRT1 in COPII vesicles and its export from the ER, although this remains
413 to be experimentally determined.

414 Besides the IRT1 interactants linked to intracellular trafficking, proteins involved in
415 metal homeostasis represent a very interesting group of candidates (Table 1). Recently,
416 coumarins, which are excreted in the rhizosphere by PDR9, were demonstrated to be
417 important for *Arabidopsis* iron acquisition by chelating Fe³⁺ and as a result facilitating iron
418 availability for FRO2 (Fourcroy et al., 2014; Fourcroy et al., 2016). Intriguingly, IRT1
419 potentially interacts with F6'H1 and Cytochrome P450/CYP82C4 that are both involved in
420 coumarin biosynthesis (Schmid et al., 2014; Rajniak et al., 2018), but the meaning of these
421 interactions remains unclear, notably because PDR9 was not identified as interacting with
422 IRT1. However, solubilization of this large transmembrane protein may not be optimal in the
423 conditions we used for the co-IP and other approaches will be necessary to determine whether
424 PDR9 and IRT1 could work in concert among a common protein complex. Interestingly,
425 FRO2 and AHA2, which act with IRT1 in the acidification-reduction-transport strategy for
426 iron acquisition, were found to interact with IRT1.

427 **IRT1, FRO2, and AHA2 form an iron-acquisition complex to optimize iron uptake in** 428 ***Arabidopsis* roots**

429 By combining co-IP analyses and split-ubiquitin assays, we showed that IRT1
430 associates with FRO2 and AHA2 proteins, but also that FRO2 and AHA2 interact together
431 (Fig. 1). Importantly, the tripartite physical interactions between IRT1, FRO2, and AHA2 are
432 direct, suggesting the existence of a dedicated protein complex at the cell surface for iron
433 uptake. Interaction between IRT1 and FRO2/AHA2 is probably not required for the intrinsic
434 activity of IRT1, since heterologous expression of IRT1 alone allows phenotypic
435 complementation of the *fet3 fet4* yeast mutant defective in iron uptake (Eide et al., 1996).
436 Similar to IRT1, FRO2 was also observed at the outer polar domain of the plasma membrane
437 in epidermal cells from the root tip (Fig. 3) and from the differentiated zone of the root
438 (Supplemental Fig. 8A). The co-polarity between FRO2 and IRT1 proteins in this domain of
439 the plasma membrane highlights the specificity of their functions achieved at the interface
440 between the root surface and the rhizosphere. On the other hand, AHA2 distribution in the
441 plasma membrane of root epidermal cells was homogenous (Fig. 3 and Supplemental Fig.
442 8B), suggesting that AHA2 does not obligatory associate with FRO2 and IRT1. This result is
443 in accordance with AHA2 function not being restricted to iron acquisition (Yuan et al., 2017;

444 Hoffmann et al., 2018; Pacifici et al., 2018). Even though the performed interaction tests do
445 not provide any information on the localization of the IRT1/FRO2/AHA2 complex, co-
446 localization analyses suggest that IRT1 may interact with FRO2 and AHA2 in the plasma
447 membrane and in endosomes (Fig. 3 and Supplemental Fig. 8). In the future, Förster
448 resonance energy transfer-fluorescence lifetime imaging microscopy (FRET-FLIM), which
449 allows the detection of protein-protein interactions in living plant cells with a high spatial and
450 temporal resolution (Zelazny et al., 2007), may reveal where IRT1 interact with FRO2 and
451 AHA2 in the cell.

452 IRT1 intracellular dynamics is regulated by ubiquitination notably in response to an
453 excess of non-iron metal substrates, following which IRT1 ubiquitination is enhanced, thus
454 triggering its endocytosis and degradation in the vacuole (Dubeaux et al., 2018). Our
455 biochemical analyses revealed that FRO2 and AHA2 are also ubiquitinated; however, their
456 ubiquitination is not modulated by the non-iron metal provision (Fig. 2 and Supplemental
457 Fig.6). This is consistent with the endocytosis of both proteins being rather constitutive and
458 not regulated by non-iron metals (Fig. 3). In this context, the ubiquitination of FRO2 and
459 AHA2 appears to be involved in a non-degradative process. First, FRO2 and AHA2 may
460 undergo mono-ubiquitination that is known to promote internalization from the cell surface
461 but to be insufficient for vacuolar targeting (Lauwers et al., 2010). Second, the internalized
462 pool of AHA2 and FRO2 may be rapidly de-ubiquitinated in endosomes allowing their
463 recycling to the plasma membrane. Third, since ubiquitination is not only involved in
464 endocytosis and degradation but is also implicated in other processes such as the allosteric
465 regulation of proteins (Komander, 2009), we may speculate that FRO2 and AHA2
466 ubiquitination may convey this type of regulation. Although the identity of the E3 ubiquitin
467 ligase at stake is unknown, IDF1 represents a possible candidate for constitutive
468 ubiquitination of AHA2 and FRO2 that will have to be tested in the future. The fact that
469 AHA2 and FRO2 likely carry out other functions independent of iron nutrition may provide
470 an explanation for their not being degraded upon non-iron metal excess. Indeed, AHA2 was
471 previously reported to contribute to acidic growth or phosphorus uptake (Yuan et al., 2017;
472 Hoffmann et al., 2018; Pacifici et al., 2018). FRO2 may play a role in copper reduction since
473 *frd1-1* mutants lack low iron-inducible copper chelate reductase activity and 35S::FRO2
474 plants display elevated copper reduction (Yi and Guerinot, 1996; Robinson et al., 1999;
475 Connolly et al., 2003). The absence of internalization of FRO2 and AHA2 from the plasma
476 membrane in root epidermal cells in response to non-iron metal excess indicates that the

477 IRT1/FRO2/AHA2 complex must disassemble prior to IRT1 endocytosis to release AHA2
478 and FRO2 pools that may engage in other processes. In response to non-iron metal excess,
479 IRT1 is phosphorylated by CIPK23 in its large cytosolic loop, boosting the interaction with
480 the E3 ubiquitin ligase IDF1 and yielding polyubiquitinated IRT1 (Dubeaux et al., 2018). We
481 demonstrated in the present study that phosphorylation of IRT1 at the same residues also
482 controls the disassembly of the root high-affinity iron uptake complex (Fig. 4).
483 Phosphorylation of IRT1 therefore has two opposite effects: dissociation of the
484 IRT1/AHA2/FRO2 complex and recruitment of IDF1. Although phosphorylation is often
485 considered as a post-translational modification allowing the recruitment of downstream
486 factors, there is mounting evidence that it also controls the disassembly of protein complexes
487 (Zhang et al., 2010; Couto et al., 2016). The fact that AHA2 and FRO2 were identified in our
488 co-IP/mass spectrometry analysis as interacting with IRT1 in non-iron metal excess is rather
489 surprising, since IRT1 phosphorylation in response to non-iron metal excess induces the
490 dissociation of the IRT1/FRO2/AHA2 complex. However, this may not induce total
491 dissociation of the complex, as evidenced by the residual interaction observed between the
492 phosphomimic IRT1 and AHA2/FRO2. This is also supported by the partial co-localization of
493 FRO2 and AHA2 with IRT1 in late endosomes under non-iron metal excess. In addition, we
494 showed that the level of co-localization between FRO2 and IRT1 in late endosomes slightly
495 increased with non-iron metal excess, suggesting that a small proportion of FRO2 is still able
496 to associate with IRT1 in these conditions. Therefore, our co-IP/mass spectrometry analysis
497 carried out when plants experience non-iron metal excess likely allowed us to identify the
498 small pool of FRO2 and AHA2 still interacting with IRT1 in endosomes. This may explain
499 why a limited number of FRO2 peptides were identified by proteomics.

500 The biological significance of iron uptake using a specific platform at the cell surface
501 is unclear but likely relies in the chemistry of iron. Although iron is abundant in most soils, its
502 bioavailability to plants is often limited. This is especially true for calcareous soils, which
503 represent one third of cultivated lands, where iron is present under the form of insoluble
504 complexes (Briat et al., 2015). During the iron-acquisition process, rhizosphere acidification
505 by the root is essential to increase iron availability, indeed the solubility of iron increases
506 1000-fold for every one unit drop in pH (Olsen et al., 1981). However, this acidification
507 process, mainly mediated by AHA2 under iron deficiency (Santi and Schmidt, 2009), is very
508 local, which likely impacts on the efficiency of iron uptake. Moreover, the presence of
509 oxygen in most soils likely provokes the rapid reoxidation of Fe^{2+} produced by FRO2 into

510 Fe^{3+} that is not transported by IRT1. Thus, we propose that the tripartite protein complex
511 gathering IRT1, FRO2, and AHA2 together creates a local environment of pH and Fe^{2+}
512 concentration in the rhizosphere that favors an optimal acquisition of iron (Fig. 4E). To
513 experimentally validate this model, mutated versions of these proteins that do not interact
514 with each other but that conserve their activities need to be generated to evaluate the
515 functional outcome on iron uptake. However, this requires deep knowledge about the
516 structure or interaction domains between these highly hydrophobic membrane proteins, which
517 is currently missing. Alternatively to the local environment theory, we can also speculate that
518 reduced iron is directly transferred from FRO2 to IRT1 by a channeling mechanism, similar
519 to what has been described for metabolic pathways. Channeling consists in the transfer of the
520 product of a proximal activity as substrate to a distal activity without equilibration with bulk
521 solvent, which increases the efficiency of the kinetic process (Kwok et al., 2006). Such
522 mechanism requires the close proximity of the donor and acceptor sites. Interestingly,
523 channeling of iron was described in yeast between the multicopper oxidase Fet3p, which
524 oxidizes Fe^{2+} to Fe^{3+} , and the iron permease Ftr1p that transports Fe^{3+} into the cells, with both
525 proteins forming a hetero-oligomeric complex (Kwok et al., 2006; Singh et al., 2006). Further
526 work will elucidate whether FRO2 and IRT1 use a similar mechanism. Whether the formation
527 of an iron-acquisition complex comprising IRT1, FRO2, and AHA2 is conserved in plants
528 other than *Arabidopsis* remains to be determined. This complex is probably not present in rice
529 (*Oryza sativa*) that combines two strategies to take up iron from the soil: a phytosiderophore-
530 based system allowing the acquisition of Fe^{3+} (Inoue et al., 2009; Lee et al., 2009) and the use
531 of Fe^{2+} transporters such as OsIRT1 (Ishimaru et al., 2006). Indeed, Fe^{3+} chelate reductase
532 activity has been shown to not be required for Fe^{2+} uptake under iron deficiency in rice,
533 suggesting that OsIRT1 works independently of OsFRO2-like proteins (Ishimaru et al., 2006).
534 In paddy fields, where rice plants are grown, Fe^{2+} is abundant due to the low redox potential
535 and therefore rice plants do not need to reduce Fe^{3+} to Fe^{2+} (Ishimaru et al., 2007). So far, the
536 description of protein complexes aimed at optimizing nutrient uptake in plant remains scarce.
537 To our knowledge, only the interaction between glutamine synthase, the principal ammonia
538 assimilatory enzyme, and the aquaglyceroporin Nodulin 26, a transporter of NH_3 , was
539 proposed to promote efficient assimilation of nitrogen in soybean (Masalkar et al., 2010).
540 Although experimental evidence is still needed, the co-localization between FRO2/AHA2 and
541 IRT1 in early endosomes in the presence of physiologically relevant levels of non-iron metals
542 suggests that the iron-acquisition complex may exist in this compartment in addition to the
543 plasma membrane (Fig.4E). This complex may help plant metal uptake by translocating iron

544 from endocytic vesicles to the cytosol. Alternatively, the AHA2/FRO2/IRT1 complex may
545 simply cycle between early endosomes and the plasma membrane in a constitutive manner or
546 in response to some undetermined stimulus. Finally, since early endosomes/trans-Golgi
547 network constitute a crossroad between endocytic and secretory pathways in plants (Dettmer
548 et al., 2006), the presence of the IRT1/FRO2/AHA2 complex in early endosomes may also
549 reflect a step in the delivery of a pre-formed complex to the plasma membrane. Future work
550 will be needed to discriminate between these different scenarios.

551

552 MATERIAL AND METHODS

553 Plant material and growth conditions

554 *Arabidopsis thaliana* wild-type (WT) plants (Col-0, Col-gl1, and Ws), the *fro2* loss-of-
555 function mutant named *frd1-1* (Robinson et al., 1999), the previously described *irt1-1*/
556 *IRT1::IRT1-mCitrine* line (Dubeaux et al., 2018), and the various transgenic plants
557 generated in this study were vertically grown in sterile conditions at 21°C with 16 h light/8 h
558 dark cycles with a light intensity of 90 $\mu\text{mol m}^{-2} \text{s}^{-1}$ using Philips 17W F17T8/TL741 bulbs.
559 The plant growth medium used was half-strength Murashige and Skoog (MS/2) medium
560 containing 1% sucrose (w/v), 1% (w/v) agar, and various concentrations of metals. Hence,
561 depending on the experiment (see below), plants were grown in the absence of iron and in the
562 presence of physiological concentrations of IRT1 secondary substrates Zn (15 μM), Mn (50
563 μM), and Co (0.05 μM) (-Fe +Metals) or in the presence of 10-fold more Zn, Mn, and Co (-Fe
564 +++Metals) corresponding to an excess of non-iron metal substrates, as previously described
565 (Dubeaux et al., 2018). Plants have also been grown in iron-replete conditions using MS/2
566 medium containing 50 μM or 100 μM Fe-EDTA (+Fe).

567 For immunopurifications followed by mass spectrometry analyses, *irt1-1/IRT1::IRT1-*
568 *mCitrine* transgenic lines and Ws WT plants were initially grown for 9 days on MS/2 medium
569 containing 50 μM Fe-EDTA, transferred for 5 days onto a -Fe +Metals medium to induce
570 IRT1-mCitrine expression, and finally subjected to a -Fe +++Metals treatment for 48 h. To
571 confirm the interactions between IRT1, FRO2, and AHA2 by co-immunopurifications, the
572 various genotypes were grown for 11 days on MS/2 medium containing 50 μM Fe-EDTA,
573 and then transferred for 4 days on a -Fe +Metals medium supplemented with 300 μM of the
574 iron chelator Ferrozine [3-(2-pyridyl)-5,6-diphenyl-1,2,4-triazine sulfonate] to ensure a rapid
575 and strong expression of genes under the control of *IRT1* and *FRO2* promoters.

576 To analyze mCherry-FRO2, AHA2-GFP, and IRT1-mCitrine ubiquitination profiles, the
577 appropriate transgenic lines as well as WT plants used as negative controls were grown for 11
578 days on -Fe +Metals MS/2 solid medium. Then, plants were transferred for 2 h in -Fe +Metals
579 (control) or -Fe +++Metals MS/2 liquid medium as previously described (Dubeaux et al.,
580 2018).

581 For microscopy analyses, transgenic lines expressing IRT1/AHA2/FRO2 fusion proteins
582 under the control of *IRT1* promoter, were first grown for 11 days on a -Fe +Metals MS/2
583 medium to ensure protein expression. Then, before observation, plants were transferred for 2
584 h in -Fe +Metals (control) or -Fe +++Metals MS/2 liquid medium. The localization of
585 mCherry-FRO2 protein in *frd1-1/FRO2::mCherry-FRO2* transgenic lines was performed on
586 plants grown for 11 days in -Fe +Metals condition.

587 For mCherry-FRO2 functionality test, *frd1-1/FRO2::mCherry-FRO2* transgenic lines, *frd1-1*
588 mutant, and Col-g11 WT plants were grown for 11 days on MS/2 lacking iron (-Fe +Metals)
589 or on MS/2 supplemented with 100 μ M Fe-EDTA (control conditions). Roots from iron-
590 starved transgenic lines and *frd1-1* (negative control) were collected to analyze mCherry-
591 FRO2 protein accumulation by Western blot analysis as detailed below.

592

593 **Constructions and generation of *Arabidopsis* transgenic lines**

594 All the constructions described in this section were obtained using the MultiSite Gateway®
595 Three-Fragment Vector Construction system. The *FRO2* promoter corresponding to a
596 sequence of 1,845 bp upstream of the *FRO2* start codon was amplified from *Arabidopsis*
597 *thaliana* genomic DNA using the attB4.promoFRO2 forward and attB1r.promoFRO2 reverse
598 primers (supplemental Table 1) and subsequently cloned into the pDONR.P4P1R entry
599 vector. The *FRO2* open reading frame (ORF) was amplified from *Arabidopsis* cDNAs with
600 the attB2r.FRO2 forward and attB3.FRO2 reverse primers (supplemental Table 1) and cloned
601 into the pDONR.P2RP3 entry vector. The *AHA2* ORF without the stop codon was amplified
602 from *Arabidopsis* cDNA with the AHA2.F forward and AHA2.R reverse primers and was
603 cloned into the pDONR.221 entry vector. The mCherry sequence without stop codon was
604 amplified with attB1.mCherry forward and attB2.mCherry reverse primers and also cloned
605 into the pDONR.221 entry vector (supplemental Table 1). Entry vectors carrying the *IRT1*
606 and *35S* promoters (pDONR.P4P1R-IRT1 and pDONR.P4P1R-35S) or the GFP and the
607 mCherry coding sequence allowing C-terminal fusions (pDONR.P2RP3-GFP and

608 pDONR.P2RP3-mCherry) were previously described (Marques-Bueno et al., 2016; Dubeaux
609 et al., 2018). Final destination vectors for expression in plants were obtained by multisite
610 Gateway® recombination using the entry vectors described above and the pH7m34GW and
611 pK7 m34GW destinations vectors used for mCherry and GFP fusions, respectively. The
612 following constructs were generated: FRO2::mCherry-FRO2, IRT1::mCherry-FRO2,
613 IRT1::AHA2-mCherry, and 35S::AHA2-GFP.

614 The previously described *irt1-1/IRT1::IRT1-mCitrine* line (Dubeaux et al., 2018) was
615 transformed with FRO2::mCherry-FRO2, IRT1::mCherry-FRO2, and IRT1::AHA2-mCherry
616 constructions by the floral-dipping technique using *Agrobacterium tumefaciens*. The *frd1-1*
617 mutant and Col-0 plants were transformed with the FRO2::mCherry-FRO2 and 35S::AHA2-
618 GFP constructs, respectively. The *irt1-1/IRT1::IRT1-mCitrine* transgenic line was crossed
619 with the Wave marker line number 25 expressing RabD1-mCherry fusion protein under the
620 control of UBQ10 promoter (Geldner et al., 2009).

621 Immunopurifications

622 Immunopurifications (IP) were performed on approximately 500 mg of *Arabidopsis* roots,
623 mostly as previously described (Dubeaux et al., 2018). Briefly, for IRT1-mCitrine IP followed
624 by mass spectrometry, for co-IP analyses between IRT1-mCitrine and mCherry-FRO2, as
625 well as for co-IP analyses between mCherry-FRO2 and endogenous AHA2, roots were
626 ground in liquid nitrogen and resuspended in IRT1 solubilization buffer (50 mM Tris-HCl
627 (pH 7.4), 150 mM NaCl, 5 mM EDTA, 1% (w/v) n-Dodecyl β-D-maltoside (DDM), and
628 plant-specific protease inhibitors (Sigma-Aldrich)). For co-IP analyses between IRT1-
629 mCitrine and endogenous AHA2, roots were ground and resuspended in RIPA buffer (50 mM
630 Tris-HCl (pH 7.5), 150 mM NaCl, 0.5% (w/v) sodium deoxycholate, 1% (v/v) IGEPAL®CA-
631 630, 0.1% (w/v) SDS, and plant-specific protease inhibitors (Sigma-Aldrich)). After two
632 successive centrifugations at $3,800 \times g$ for 10 min at 4°C, the resultant supernatants were
633 collected and solubilization of membrane proteins was continued for 1 h 30 min at 4°C on a
634 rotating wheel. Samples were then centrifuged at $100,000 \times g$ for 1 h at 4°C to remove
635 unsolubilized material and supernatants containing solubilized proteins were recovered for
636 IPs. This ultracentrifugation step avoids the immuno-capture of proteins present in patches of
637 residual non-solubilized membranes, allowing the IP to be carried out on solubilized protein
638 complexes only. IPs of GFP and mCitrine fusion proteins were performed using μMACS GFP
639 isolation kit (Miltenyi Biotec) whereas IP of mCherry fusion proteins was performed using

640 RFP-Trap®_MA magnetic beads (Chromotek), following the instructions of the
641 manufacturers. Before elution, extensive washes were performed with IRT1 solubilization
642 buffer or RIPA buffer depending on the IP type. Co-IP analyses followed by mass
643 spectrometry were performed twice. Co-IP combined with immunodetections were performed
644 thrice with similar results.

645 To analyze the ubiquitination profile of AHA2-GFP and IRT1-mCitrine, the solubilization of
646 fusion proteins as well as the IP procedure were performed exactly as previously described
647 (Dubeaux et al., 2018). The same protocol was used for mCherry-FRO2 except that the
648 protein was immunopurified with RFP-Trap®_MA magnetic beads (Chromotek). Three
649 independent analyses of ubiquitination profiles were performed.

650 **Mass spectrometry analysis**

651 For sample preparation, proteins from each eluate were separated by SDS-PAGE in order to
652 fractionate the protein samples into two fractions, including proteins 10–63 kDa and above 63
653 kDa, respectively, to exclude abundant contaminating IRT1-mCitrine protein at 63 kDa. After
654 Coomassie-Blue staining, each gel fraction was cut into bands and subjected to in-gel trypsin
655 digestion with the Progest robot (Genomic Solutions) using standard conditions including
656 reduction and alkylation as described previously (Blanchet et al., 2014). Tryptic peptides
657 extracted from the different bands of each gel fraction were pooled, vacuum dried, and
658 resuspended in 0.1% (v/v) formic acid prior to nanoLC-MS/MS mass spectrometry analyzes.
659 The same cutting pattern of the SDS-PAGE lane was performed for each eluate.

660 Tryptic peptides from the two or three SDS-PAGE fractions from each eluate were analyzed
661 separately by nanoLC-MS/MS with the Triple-TOF 4600 mass spectrometer (ABSciex)
662 coupled to the nanoRSLC ultra performance liquid chromatography (UPLC) system (Thermo
663 Scientific) equipped with a trap column (Acclaim PepMap100C18, 75 μ m.i.d. \times 2 cm, 3 μ m)
664 and an analytical column (Acclaim PepMapRSLCC18, 75 μ m.i.d. \times 50 cm, 2 μ m, 100 Å).
665 Peptides were loaded at 5 μ l/min with 0.05% (v/v) TFA in 5% (v/v) acetonitrile and peptide
666 separation was performed at a flow rate of 300 nl/min with a 5–35% (v/v) solvent B gradient
667 in 40 min. Solvent A was 0.1% (v/v) formic acid in water, and solvent B was 0.1% (v/v)
668 formic acid in 100% acetonitrile. NanoLC-MS/MS experiments were conducted in a Data
669 Dependent acquisition method by selecting the 20 most intense precursors for CID
670 fragmentation with Q1 quadrupole set at low resolution for better sensitivity.

671 Protein identification was performed by processing raw data with MS Data Converter
672 software (AB Sciex) for generating .mgf data files and protein identification were performed
673 using the MASCOT search engine (Matrix science, London, UK) against the Swissprot and
674 TAIR10 databases with carbamidomethylation of cysteines set as fixed modification and
675 oxidation of methionines as variable modifications. Peptide and fragment tolerance were set
676 at 20 ppm and 0.05 Da, respectively. Results were analyzed with Scaffold 3.6.5 software
677 (Proteome Software). Proteins were validated when identified with at least two unique
678 peptides and 95% probability levels for both peptides and proteins.

679

680 **Extraction of total proteins and immunoblots**

681 Total proteins were extracted from around 100 mg of *Arabidopsis* roots ground in liquid
682 nitrogen and directly resuspended in 2X SDS sample buffer. Samples were heated at 65°C for
683 10 min, centrifuged 10 min at 20,000 × g and finally supernatants were collected and directly
684 used for SDS-PAGE. Protein extraction from yeast was carried out as previously described
685 (von der Haar, 2007).

686 Immunoblot analyses were performed as previously described (Barberon et al., 2011).
687 Immunodetection of GFP and mCitrine fusion proteins was performed using an anti-GFP
688 antibody conjugated to horseradish peroxidase (HRP) (Miltenyi Biotec 130-091-833,
689 1/5,000). mCherry fusion proteins were monitored with a rabbit anti-DsRed antibody
690 (Clontech 632496, 1/5,000). Endogenous AHA2 protein was immunodetected using a rabbit
691 antibody initially raised against the Plasma Membrane H⁺-ATPase 2 (PMA2) from *Nicotiana*
692 *plumbaginifolia* (W1C) diluted 1/15,000 (Morsomme et al., 1998). Ubiquitin modifications
693 were detected with the P4D1 mouse anti-ubiquitin antibody (Millipore 05-944, 1/4,000). The
694 detection of NubG-IRT1 protein from yeast used anti-HA antibodies (Miltenyi Biotec 130-
695 091-972, 1/7,000). Anti-tubulin antibodies were used as loading control (Agrisera AS10 681,
696 1/5,000). The anti-rabbit IgG or anti-mouse IgG secondary antibodies coupled to HRP were
697 both diluted 1/20,000. Detection of HRP chemiluminescence was performed using
698 SuperSignal West Dura Extended Duration Substrate (Thermo Scientific) in a Chemidoc
699 Touch Imaging system (Bio-Rad). Stain-Free protein staining (Bio-Rad) was used as a
700 loading control as previously described (Dubeaux et al., 2018). To quantify IRT1-mCitrine,
701 AHA2-GFP, and mCherry-FRO2 ubiquitination levels under different metal regimes, signal
702 intensity observed with anti-ubiquitin immunoblots performed on IRT1-mCitrine, AHA2-

703 GFP, or mCherry-FRO2 immunopurified proteins was measured using Image Lab 6.0.1 and
704 normalized to the quantity of immunopurified proteins detected in IP with anti-GFP or anti-
705 DsRed antibodies. To facilitate comparisons, the ubiquitination level measured in the
706 presence of physiological concentrations of non-iron metal substrates was arbitrary fixed to 1.

707

708 **Constructions and split-ubiquitin assay**

709 Split-ubiquitin vectors were generated using the Gateway® technology. First, the *FRO2* ORF
710 without the stop codon and the *AHA2* ORF with the stop codon were amplified with
711 *FRO2.F/FRO2.R* and *AHA2.F/AHA2stop.R* primers, respectively (supplemental Table 1),
712 and were both cloned into the pDONR.221 entry vector. pDONR.221-BRI1 without stop was
713 previously generated (Martins et al., 2015) and pDONR.221-AHA2 without stop was created
714 in this study as mentioned above. Then, *FRO2*, *AHA2*, and *BRI1* ORFs without the stop codon
715 were inserted into pMetYC-DEST destination vector (Hachez et al., 2014) to produce
716 methionine-repressible constructs *FRO2-Cub-PLV*, *AHA2-Cub-PLV*, and *BRI1-Cub-PLV*,
717 respectively, where Cub corresponds to the C-terminal part of ubiquitin and PLV to a
718 chimeric transcription factor. *AHA2* ORF with the stop codon was cloned into the pNX35-
719 DEST destination vector to generate the NubG-*AHA2* fusion wherein NubG corresponds to
720 the mutated N-terminal part of ubiquitin. The NubG-IRT1, NubG-IRT1_{S/TxD}, and NubG-
721 IRT1_{S/TxA} constructs were previously described (Dubeaux et al., 2018). It is important to note
722 that NubG and Cub were fused to a cytosolic part of IRT1, *FRO2*, *AHA2*, and *BRI1*,
723 according to the known or predicted topology of these proteins. The wild-type ubiquitin N-
724 terminal fragment (NubWT) expressed by the pNubWT-Xgate vector and the NubG fragment
725 expressed by the non-recombined pNX35-DEST vector were used as a positive and negative
726 control, respectively (Hachez et al., 2014).

727 Split-ubiquitin assay was performed as previously described (Dubeaux et al., 2018). Briefly,
728 THY.AP4 yeast strain was co-transformed with the Nub and Cub constructs of interest and
729 co-transformed cells were selected on SD medium lacking Leu and Trp. Then, yeast co-
730 expressing Cub-PLV fusion proteins with NubG fusion proteins or NubG (negative control of
731 interaction) or NubWT (positive control of interaction) were dropped in serial dilutions (O.D.
732 1, 0.1, 0.01) onto SD medium without Leu and Trp (control medium) or onto SD medium
733 lacking Leu, Trp, His, Ade (selective medium) supplemented with 500 µM methionine (250
734 µM methionine for IRT1/BRI1 interaction test) to limit the expression of the Cub-PLV fusion

735 proteins. Yeast growth on control and selective medium was recorded after 24 h and 48 h at
736 30°C, respectively. Besides internal negative interaction tests performed by co-expressing
737 Cub-PLV fusion proteins with NubG, co-expression of NubG-IRT1 and BRI1-Cub-PLV was
738 used as an additional negative control. Quantification of interactions were carried out using
739 liquid yeast cultures and by measuring O.D. over time. Three independent split-ubiquitin
740 interaction tests were performed with similar results.

741 **Confocal microscopy**

742 Microscopy was performed with a Leica SP8 upright confocal laser scanning microscope. For
743 mCitrine and mCherry imaging, the 514-nm and 561-nm lasers were used, respectively.
744 Before observation, plants were mounted in MS/2 liquid medium containing the proper metal
745 composition (-Fe +Metals or -Fe +++ Metals). Representative images are shown. For
746 quantifications, z-stacks encompassing the whole cell volume were imaged and then subjected
747 to maximum projection. The Mander's coefficient (M2) of mCherry-FRO2 and AHA2-
748 mCherry endosomal structures showing overlap with IRT1-mCitrine labeled endosomes were
749 determined using the ImageJ plugin Coloc2. 27 cells (3 independent cells from 3 different
750 plants among 3 independent experiments) were analyzed for each condition and genotype.
751 The M2 coefficient is the ratio of the summed intensities of pixels from the red image, for
752 which the intensity in the green channel is above zero, to the total intensity in the red channel.
753 M2 coefficients vary from 0 to 1, the former value corresponding to non-overlapping
754 endosomes and the latter reflecting 100% co-localization between both channels. A ratio of
755 0.5 indicates a 50% overlap between the two channels. Here, we used M2 to reflect the co-
756 localization between mCherry-FRO2 and IRT1-mCitrine, or AHA2-mCherry and IRT1-
757 mCitrine. An unpaired *t*-test was used to determine whether the overlapping was different in
758 response to metal excess (-Fe +++Metals). The ratios of plasma membrane over intracellular
759 signal content were obtained by selecting whole-cell and intracellular content mean
760 fluorescence with ImageJ.

761

762 **Statistical analyses**

763 For confocal microscopy experiments, a representative image is shown. Statistical analyses
764 were performed using the software GraphPad Prism 7. The sample size and statistical tests
765 used are mentioned in the figure legends.

766

767 **Accession numbers**

768 Sequence data from this article can be found in the GenBank/EMBL data libraries under
769 accession numbers: *IRT1* (AT4G19690), *FRO2* (AT1G01580), *AHA2* (AT4G30190), and
770 *BRI1* (AT4G39400).

771 **Supplemental Data**

772 **Supplemental Figure S1.** Immunopurification of IRT1-mCitrine and the associated proteins.

773

774 **Supplemental Figure S2.** Expression of mCherry-FRO2 complements the *frd1-1* mutant
775 phenotype in iron-deficient conditions.

776

777 **Supplemental Figure S3.** IRT1-mCitrine and RabD1-mCherry co-localize in early
778 endosomes in *Arabidopsis* root epidermal cells.

779

780 **Supplemental Figure S4.** mCherry-FRO2 protein is not cross-immunopurified with anti-GFP
781 antibody.

782

783 **Supplemental Figure S5.** FRO2 and AHA2 interact in *Arabidopsis* root cells.

784

785 **Supplemental Figure S6.** FRO2 and AHA2 are ubiquitinated in *Arabidopsis* root cells in a
786 metal-independent manner, replicate.

787

788 **Supplemental Figure S7.** Phosphomimic and non-phosphorylatable mutations in IRT1 do
789 not influence IRT1 protein accumulation in yeast.

790

791 **Supplemental Figure S8.** Co-localization of IRT1 and FRO2/AHA2 in differentiated root
792 cells.

793

794 **Supplemental Table S1.** List of primers used in this study.

795

796 **Supplemental Dataset S1.** IRT1 interactome determined by co-immunopurification of IRT1-
797 mCitrine combined with mass spectrometry analyses.

799 **ACKNOWLEDGMENTS**

800 We thank Marc Boutry for the anti-PMA2 antibody, Mary Lou Guerinot for providing the
 801 *frd1-1* mutant, François Chaumont for the split-ubiquitin vectors, and Alexandre Martinière
 802 and Alexander Johnson for their help in image analysis. We also thank Sébastien Thomine for
 803 interesting scientific discussions. This work has benefited from the facilities and expertise of
 804 the I2BC proteomic platform SICaPS, supported by IBSA, Ile de France Region, Plan
 805 Cancer, CNRS and Paris-Sud University and the expertise of David Cornu. The present study
 806 has also benefited from Imagerie-Gif core facility supported by Agence Nationale de la
 807 Recherche (ANR-11-EQPX-0029/Morphoscope, ANR-10-INBS-04/FranceBioImaging;
 808 ANR-11-IDEX-0003-02/ Saclay Plant Sciences).

809 **Tables**

810 **Table 1.** IRT1 interactants involved in intracellular trafficking or metal homeostasis.

811 Among the 142 putative IRT1 interacting-proteins identified by co-IP combined with mass
 812 spectrometry, we present in this table proteins that are associated to intracellular trafficking or
 813 metal homeostasis according to Gene Ontology (GO) annotations from The Arabidopsis
 814 Information resource (TAIR) (<https://www.arabidopsis.org>). The maximum number of unique
 815 peptides identified for each protein from the two independent experiments (see Supplemental
 816 Dataset S1) is indicated.

	Accession	Protein name	Maximum number of unique peptides
Intracellular trafficking	AT3G11130	Clathrin heavy chain	24
	AT1G04820	Tubulin alpha-4 chain	6
	AT1G29310	SecY protein transport family protein	2
	AT5G09810	Actin 7	4
	AT4G33650	Dynammin-related protein 3A	2
	AT3G63460	SEC31b, COPII component	6
	AT4G18800	RAB GTPase homolog A1D	3
	AT1G62020	Coatomer alpha subunit, COPI component	2
	AT4G31480	Coatomer beta subunit, COPI component	2
	AT4G17530	RAB GTPase homolog 1C	2
	AT1G49240	Actin 8	2
	AT5G05010	Clathrin adaptor complexes medium subunit family protein	2
	AT2G21390	Coatomer, alpha subunit, COPI component	2
	AT5G44340	Tubulin beta chain 4	2
	AT2G30050	SEC13a, COPII component	2
	M	AT4G30190	H(+)-ATPase 2

AT4G31940	Cytochrome P450 / CYP82C4	3
AT3G13610	Feruloyl-Coenzyme A 6'-Hydroxylase 1 (F6'H1)	2
AT4G27860	Vacuolar iron transporter (VIT) family protein	11
AT5G24290	Vacuolar iron transporter (VIT) family protein	8
AT2G01530	MLP-like protein 329	5
AT1G59870	Pleiotropic drug resistance 8 / Penetration 3	4
AT1G01580	Ferric Reduction Oxidase 2	3
AT1G07890	Ascorbate peroxidase 1	2

817

818

819 **Figure Legends**

820 **Figure 1. FRO2 and AHA2 are part of an IRT1-protein complex.**

821 **(A)** Endogenous AHA2 is co-immunopurified with IRT1-mCitrine in *Arabidopsis* root cells.
 822 Immunopurifications (IP) were performed using anti-GFP antibodies on solubilized root
 823 protein extracts from *irt1-1/IRT1::IRT1-mCitrine* and wild-type plants (negative control).
 824 Inputs and IP fractions were subjected to immunoblotting (IB) with anti-GFP (top) and anti-
 825 AHA/PMA2 antibodies (bottom).

826 **(B)** mCherry-FRO2 is co-immunopurified with IRT1-mCitrine in *Arabidopsis* root cells. IP
 827 were performed using anti-GFP antibodies on solubilized root protein extracts from *irt1-1/IRT1::IRT1-mCitrine*
 828 plants co-expressing FRO2::mCherry-FRO2 or UBQ10::RabD1-
 829 mCherry, this protein co-localizing with IRT1 in endosomes (negative control). Inputs and IP
 830 fractions were subjected to IB with anti-GFP (top) and anti- mCherry antibodies (bottom).
 831 Note that mCherry-FRO2 migrates at the expected size (top band) but also at a lower
 832 molecular weight (bottom band). For the co-IP experiments in (A) and (B), roots were
 833 harvested from plants grown for 11 days on MS/2 medium containing 50 μ M Fe-EDTA, and
 834 then transferred for 4 days on MS/2 medium lacking iron and supplemented with 300 μ M of
 835 the iron chelator Ferrozine, in the presence of physiologically relevant concentrations of non-
 836 iron metal substrates. Representative immunoblots are shown.

837 **(C)** IRT1 directly interacts with FRO2 and AHA2 in a split-ubiquitin assay. Yeasts co-
 838 expressing Cub-PLV fusion proteins with NubG fusion proteins or NubG (negative control of
 839 interaction) or NubWT (positive control of interaction) were dropped in serial dilutions on a
 840 synthetic medium without Leu and Trp (control medium) or without Leu, Trp, His, Ade
 841 (selective medium). For the interaction tests between IRT1, FRO2, and AHA2, yeast growth
 842 on control and selective media was recorded after 24h and 48h, respectively. Besides internal

843 negative interaction tests performed by co-expressing Cub fusion proteins with NubG, an
844 additional negative control was introduced in this assay by co-expressing NubG-IRT1 and
845 BRI1-Cub. For this IRT1-BRI1 interaction test, yeast growth on control and selective media
846 was recorded after 48h and 72h, respectively. OD: optical density. A representative assay is
847 shown.

848

849

850 **Figure 2. FRO2 and AHA2 are ubiquitinated in *Arabidopsis* root cells in a metal-**
851 **independent manner.**

852 Immunopurifications (IP) were performed using anti-GFP antibodies on solubilized root
853 protein extracts from wild-type, *irt1-1/IRT1::IRT1-mCitrine* and *Col0/35S::AHA2-GFP* plants
854 (A) or using anti-mCherry antibodies on solubilized root protein extracts from wild-type and
855 *frd1/FRO2::mCherry-FRO2* plants (B). Inputs and IP fractions were subjected to
856 immunoblotting (IB) with anti-Ub antibody (P4D1) (A and B, top), anti-GFP (A, bottom), or
857 anti-mCherry antibodies (B, bottom). Non-ubiquitinated and ubiquitinated forms of the
858 studied proteins are indicated by an arrow and a bar (-Ub_n), respectively. Roots were
859 harvested from plants grown for 11 days on MS/2 medium lacking iron (-), in the presence of
860 physiologically relevant concentrations of non-iron metal substrates (+), and then transferred
861 for 2 hours to the same medium (control) or to a medium lacking iron and containing an
862 excess of non-iron metals (+++). Wild-type plants were used as negative controls for IP. In
863 (A), due to very low expression level, AHA2-GFP is not detected in inputs but solely in IP
864 fractions after enrichment.

865 (C) Quantification of IRT1-mCitrine, AHA2-GFP, and mCherry-FRO2 ubiquitination in the
866 presence of physiologically relevant concentrations of non-iron metal substrates (+) or an
867 excess of these metals (+++). The intensity of the ubiquitin signal from IRT1-mCitrine,
868 AHA2-GFP, and mCherry-FRO2 IP shown in (A) and (B) was measured using Image Lab
869 and normalized to the quantity of immunopurified proteins. Results are shown as ratio relative
870 to the (+) condition for each protein to reveal the influence of metal treatment.

871

872 **Figure 3. The endocytosis of IRT1 and FRO2/AHA2 is differentially regulated by non-**
873 **iron metal substrates in root tip epidermal cells.**

874 Confocal microscopy analyses of root epidermal cells from *irt1-1/IRT1::IRT1-mCitrine* plants
875 co-expressing IRT1::mCherry-FRO2 (**A, left panel**) or IRT1::AHA2-mCherry (**B, left panel**).
876 Plants were grown for 11 days on MS/2 medium lacking iron, in the presence of
877 physiologically relevant concentrations of non-iron metal substrates, and then transferred for
878 2 hours to the same medium (-Fe +Metals, control) or to a medium lacking iron and
879 containing an excess of non-iron metals (-Fe +++Metals). To standardize microscopy analysis
880 at the root tip, the same cells located just above the lateral root cap were systematically
881 analyzed. Scale bars, 10 μ m. Representative images are shown. Right panels in (**A**) and (**B**)
882 show the ratio of plasma membrane to intracellular signal intensities for IRT1-mCitrine,
883 mCherry-FRO2, and AHA2-mCherry from experiments performed as in the left panels of (**A**)
884 and (**B**).

885 Mander's coefficients (M2) of mCherry-FRO2 (**C**) and AHA2-mCherry (**D**) endosomal
886 structures showing overlap with IRT1-mCitrine labeled endosomes were calculated from
887 experiments performed as in (**A**) and (**B**), left panels. All the quantifications shown in this
888 figure were carried out in triplicates on stacks encompassing epidermal cells. In total, 27 cells
889 were analyzed for each condition and genotype. Error bars represent SD (n = 27) for each
890 genotype. The asterisks indicate significant differences to -Fe +Metals (unpaired t-test, p <
891 0.0001).

892

893 **Figure 4. Phosphorylation of IRT1 decreases its interaction with AHA2 and FRO2.**
894 **Tentative model for the functioning of the iron-acquisition complex.**

895 (**A-D**) Effect of IRT1 phospho-status on its interaction with AHA2 and FRO2. Split-ubiquitin
896 interaction tests were performed between wild-type IRT1, IRT1 variants for phosphorylation
897 sites (phosphomimic S/TxD and non-phosphorylatable S/TxA) and AHA2 (**A**), or FRO2 (**B**).
898 Yeasts were dropped in serial dilutions on a synthetic medium without Leu and Trp (control
899 medium) or without Leu, Trp, His, Ade (selective medium). NubG and NubWT were used as
900 negative and positive controls of interaction, respectively. Yeast growth on control and
901 selective medium was monitored after 48h and 72h, respectively. O.D: optical density.
902 Representative assays are shown. To quantify interactions, the same tests were performed in
903 liquid cultures as shown in (**C**) and (**D**). The O.D measured for transformed yeast grown in
904 the selective medium for 24h was normalized to the O.D measured for the same yeast grown

905 in the control medium for 16h (relative growth). Error bars represent SEM, n = 8 in (C) and n
906 = 12 in (D).

907 **(E)** Putative functioning of the iron-acquisition complex. IRT1, FRO2, and AHA2 proteins
908 interact at the outer polar plasma membrane (PM) domain of root epidermal cells to form a
909 specialized complex that likely optimizes iron acquisition by creating a local environment
910 with low pH and high Fe²⁺ concentration. Outside this optimal zone for iron acquisition, we
911 propose that Fe²⁺ is constantly re-oxidized to Fe³⁺, which in turn forms insoluble iron
912 complexes. In addition to be plasma membrane localized, the iron-acquisition complex is also
913 probably present in early endosomes, reflecting endocytic events of the complex. Note that
914 contrary to IRT1 and FRO2, AHA2 is distributed at both plasma membrane polar domains.
915 FRO2 might be not exclusively associated with IRT1. This model depicts the localization of
916 IRT1, FRO2, and AHA2 in the absence of iron and in the presence of physiologically relevant
917 concentrations of non-iron metal substrates (-Fe +Metals). Although IRT1, FRO2, and AHA2
918 interact all together, this feature is not represented to simplify the scheme.

919

920 LITERATURE CITED

- 921 **Barberon M, Dubeaux G, Kolb C, Isono E, Zelazny E, Vert G** (2014) Polarization of IRON-REGULATED
922 TRANSPORTER 1 (IRT1) to the plant-soil interface plays crucial role in metal homeostasis.
923 Proc Natl Acad Sci U S A **111**: 8293-8298
- 924 **Barberon M, Zelazny E, Robert S, Conejero G, Curie C, Friml J, Vert G** (2011) Monoubiquitin-
925 dependent endocytosis of the iron-regulated transporter 1 (IRT1) transporter controls iron
926 uptake in plants. Proc Natl Acad Sci U S A **108**: E450-458
- 927 **Bellati J, Champeyroux C, Hem S, Rofidal V, Krouk G, Maurel C, Santoni V** (2016) Novel Aquaporin
928 Regulatory Mechanisms Revealed by Interactomics. Mol Cell Proteomics **15**: 3473-3487
- 929 **Blanchet S, Cornu D, Argentini M, Namy O** (2014) New insights into the incorporation of natural
930 suppressor tRNAs at stop codons in Saccharomyces cerevisiae. Nucleic Acids Res **42**: 10061-
931 10072
- 932 **Briat JF, Dubos C, Gaymard F** (2015) Iron nutrition, biomass production, and plant product quality.
933 Trends Plant Sci **20**: 33-40
- 934 **Chung KP, Zeng Y, Jiang L** (2016) COPII Paralogs in Plants: Functional Redundancy or Diversity?
935 Trends Plant Sci **21**: 758-769
- 936 **Cointry V, Vert G** (2019) The bifunctional transporter-receptor IRT1 at the heart of metal sensing and
937 signalling. New Phytol **223**: 1173-1178
- 938 **Colangelo EP, Gueriot ML** (2004) The essential basic helix-loop-helix protein FIT1 is required for the
939 iron deficiency response. Plant Cell **16**: 3400-3412
- 940 **Connolly EL, Campbell NH, Grotz N, Prichard CL, Gueriot ML** (2003) Overexpression of the FRO2
941 ferric chelate reductase confers tolerance to growth on low iron and uncovers
942 posttranscriptional control. Plant Physiol **133**: 1102-1110
- 943 **Couto D, Niebergall R, Liang X, Bucherl CA, Sklenar J, Macho AP, Ntoukakis V, Derbyshire P,
944 Altenbach D, Maclean D, Robatzek S, Uhrig J, Menke F, Zhou JM, Zipfel C** (2016) The

945 Arabidopsis Protein Phosphatase PP2C38 Negatively Regulates the Central Immune Kinase
946 BIK1. *PLoS Pathog* **12**: e1005811

947 **Dettmer J, Hong-Hermesdorf A, Stierhof YD, Schumacher K** (2006) Vacuolar H⁺-ATPase activity is
948 required for endocytic and secretory trafficking in Arabidopsis. *Plant Cell* **18**: 715-730

949 **Dubeaux G, Neveu J, Zelazny E, Vert G** (2018) Metal Sensing by the IRT1 Transporter-Receptor
950 Orchestrates Its Own Degradation and Plant Metal Nutrition. *Mol Cell* **69**: 953-964 e955

951 **Eide D, Broderius M, Fett J, Guerinot ML** (1996) A novel iron-regulated metal transporter from plants
952 identified by functional expression in yeast. *Proceedings of the National Academy of Sciences*
953 of the United States of America **93**: 5624-5628

954 **Fan L, Li R, Pan J, Ding Z, Lin J** (2015) Endocytosis and its regulation in plants. *Trends Plant Sci* **20**:
955 388-397

956 **Fourcroy P, Siso-Terraza P, Sudre D, Saviron M, Reyt G, Gaymard F, Abadia A, Abadia J, Alvarez-
957 Fernandez A, Briat JF** (2014) Involvement of the ABCG37 transporter in secretion of
958 scopoletin and derivatives by Arabidopsis roots in response to iron deficiency. *New Phytol*
959 **201**: 155-167

960 **Fourcroy P, Tissot N, Gaymard F, Briat JF, Dubos C** (2016) Facilitated Fe Nutrition by Phenolic
961 Compounds Excreted by the Arabidopsis ABCG37/PDR9 Transporter Requires the IRT1/FRO2
962 High-Affinity Root Fe(2+) Transport System. *Mol Plant* **9**: 485-488

963 **Gao C, Luo M, Zhao Q, Yang R, Cui Y, Zeng Y, Xia J, Jiang L** (2014) A unique plant ESCRT component,
964 FREE1, regulates multivesicular body protein sorting and plant growth. *Curr Biol* **24**: 2556-
965 2563

966 **Geldner N, Denervaud-Tendon V, Hyman DL, Mayer U, Stierhof YD, Chory J** (2009) Rapid,
967 combinatorial analysis of membrane compartments in intact plants with a multicolor marker
968 set. *Plant J* **59**: 169-178

969 **Hachez C, Laloux T, Reinhardt H, Cavez D, Degand H, Grefen C, De Rycke R, Inze D, Blatt MR,
970 Russinova E, Chaumont F** (2014) Arabidopsis SNAREs SYP61 and SYP121 coordinate the
971 trafficking of plasma membrane aquaporin PIP2;7 to modulate the cell membrane water
972 permeability. *Plant Cell* **26**: 3132-3147

973 **Haruta M, Tan LX, Bushey DB, Swanson SJ, Sussman MR** (2018) Environmental and Genetic Factors
974 Regulating Localization of the Plant Plasma Membrane H(+)-ATPase. *Plant Physiol* **176**: 364-
975 377

976 **Hoffmann RD, Olsen LI, Ezike CV, Pedersen JT, Manstretta R, Lopez-Marques RL, Palmgren M** (2018)
977 Roles of plasma membrane proton ATPases AHA2 and AHA7 in normal growth of roots and
978 root hairs in Arabidopsis thaliana. *Physiol Plant*

979 **Inoue H, Kobayashi T, Nozoye T, Takahashi M, Kakei Y, Suzuki K, Nakazono M, Nakanishi H, Mori S,
980 Nishizawa NK** (2009) Rice OsYSL15 is an iron-regulated iron(III)-deoxymugineic acid
981 transporter expressed in the roots and is essential for iron uptake in early growth of the
982 seedlings. *J Biol Chem* **284**: 3470-3479

983 **Ishimaru Y, Kim S, Tsukamoto T, Oki H, Kobayashi T, Watanabe S, Matsushashi S, Takahashi M,
984 Nakanishi H, Mori S, Nishizawa NK** (2007) Mutational reconstructed ferric chelate reductase
985 confers enhanced tolerance in rice to iron deficiency in calcareous soil. *Proc Natl Acad Sci U S*
986 *A* **104**: 7373-7378

987 **Ishimaru Y, Suzuki M, Tsukamoto T, Suzuki K, Nakazono M, Kobayashi T, Wada Y, Watanabe S,
988 Matsushashi S, Takahashi M, Nakanishi H, Mori S, Nishizawa NK** (2006) Rice plants take up
989 iron as an Fe³⁺-phytosiderophore and as Fe²⁺. *Plant J* **45**: 335-346

990 **Ivanov R, Brumbarova T, Blum A, Jantke AM, Fink-Straube C, Bauer P** (2014) SORTING NEXIN1 Is
991 Required for Modulating the Trafficking and Stability of the Arabidopsis IRON-REGULATED
992 TRANSPORTER1. *Plant Cell* **26**: 1294-1307

993 **Jakoby M, Wang HY, Reidt W, Weisshaar B, Bauer P** (2004) FRU (BHLH029) is required for induction
994 of iron mobilization genes in Arabidopsis thaliana. *FEBS Lett* **577**: 528-534

995 **Jeong J, Merkovich A, Clyne M, Connolly EL** (2017) Directing iron transport in dicots: regulation of
996 iron acquisition and translocation. *Curr Opin Plant Biol* **39**: 106-113

- 997 **Johnson A, Vert G** (2016) Unraveling K63 Polyubiquitination Networks by Sensor-Based Proteomics.
998 *Plant Physiol* **171**: 1808-1820
- 999 **Karlova R, Boeren S, Russinova E, Aker J, Vervoort J, de Vries S** (2006) The Arabidopsis SOMATIC
1000 EMBRYOGENESIS RECEPTOR-LIKE KINASE1 protein complex includes BRASSINOSTEROID-
1001 INSENSITIVE1. *Plant Cell* **18**: 626-638
- 1002 **Khan I, Gratz R, Denezhkin P, Schott-Verdugo SN, Angrand K, Genders L, Basgaran RM, Fink-Straube
1003 C, Brumbarova T, Gohlke H, Bauer P, Ivanov R** (2019) Calcium-promoted interaction
1004 between the C2-domain protein EHB1 and metal transporter IRT1 inhibits Arabidopsis iron
1005 acquisition. *Plant Physiol*
- 1006 **Kim DY, Bovet L, Maeshima M, Martinoia E, Lee Y** (2007) The ABC transporter AtPDR8 is a cadmium
1007 extrusion pump conferring heavy metal resistance. *Plant J* **50**: 207-218
- 1008 **Kim DY, Scalf M, Smith LM, Vierstra RD** (2013) Advanced proteomic analyses yield a deep catalog of
1009 ubiquitylation targets in Arabidopsis. *Plant Cell* **25**: 1523-1540
- 1010 **Komander D** (2009) The emerging complexity of protein ubiquitination. *Biochem Soc Trans* **37**: 937-
1011 953
- 1012 **Kwok EY, Severance S, Kosman DJ** (2006) Evidence for iron channeling in the Fet3p-Ftr1p high-
1013 affinity iron uptake complex in the yeast plasma membrane. *Biochemistry* **45**: 6317-6327
- 1014 **Lauwers E, Erpapazoglou Z, Haguenaer-Tsapis R, Andre B** (2010) The ubiquitin code of yeast
1015 permease trafficking. *Trends Cell Biol* **20**: 196-204
- 1016 **Lee S, Chiecko JC, Kim SA, Walker EL, Lee Y, Guerinot ML, An G** (2009) Disruption of OsYSL15 leads
1017 to iron inefficiency in rice plants. *Plant Physiol* **150**: 786-800
- 1018 **Marques-Bueno MDM, Morao AK, Cayrel A, Platre MP, Barberon M, Caillieux E, Colot V, Jaillais Y,
1019 Roudier F, Vert G** (2016) A versatile Multisite Gateway-compatible promoter and transgenic
1020 line collection for cell type-specific functional genomics in Arabidopsis. *Plant J* **85**: 320-333
- 1021 **Martins S, Dohmann EM, Cayrel A, Johnson A, Fischer W, Pojer F, Satiat-Jeunemaitre B, Jaillais Y,
1022 Chory J, Geldner N, Vert G** (2015) Internalization and vacuolar targeting of the
1023 brassinosteroid hormone receptor BRI1 are regulated by ubiquitination. *Nat Commun* **6**:
1024 6151
- 1025 **Masalkar P, Wallace IS, Hwang JH, Roberts DM** (2010) Interaction of cytosolic glutamine synthetase
1026 of soybean root nodules with the C-terminal domain of the symbiosome membrane nodulin
1027 26 aquaglyceroporin. *J Biol Chem* **285**: 23880-23888
- 1028 **Morsomme P, Dambly S, Maudoux O, Boutry M** (1998) Single point mutations distributed in 10
1029 soluble and membrane regions of the *Nicotiana plumbaginifolia* plasma membrane PMA2
1030 H⁺-ATPase activate the enzyme and modify the structure of the C-terminal region. *J Biol
1031 Chem* **273**: 34837-34842
- 1032 **Olsen RA, Clark RB, Bennett JH** (1981) THE ENHANCEMENT OF SOIL FERTILITY BY PLANT-ROOTS.
1033 *American Scientist* **69**: 378-384
- 1034 **Pacifici E, Di Mambro R, Dello Iorio R, Costantino P, Sabatini S** (2018) Acidic cell elongation drives cell
1035 differentiation in the Arabidopsis root. *EMBO J* **37**
- 1036 **Palmer CM, Guerinot ML** (2009) Facing the challenges of Cu, Fe and Zn homeostasis in plants. *Nat
1037 Chem Biol* **5**: 333-340
- 1038 **Qi X, Zheng H** (2013) Rab-A1c GTPase defines a population of the trans-Golgi network that is
1039 sensitive to endosidin1 during cytokinesis in Arabidopsis. *Mol Plant* **6**: 847-859
- 1040 **Rajniak J, Giehl RFH, Chang E, Murgia I, von Wiren N, Sattely ES** (2018) Biosynthesis of redox-active
1041 metabolites in response to iron deficiency in plants. *Nat Chem Biol* **14**: 442-450
- 1042 **Robinson NJ, Procter CM, Connolly EL, Guerinot ML** (1999) A ferric-chelate reductase for iron uptake
1043 from soils. *Nature* **397**: 694-697
- 1044 **Rodriguez-Celma J, Lin WD, Fu GM, Abadia J, Lopez-Millan AF, Schmidt W** (2013) Mutually exclusive
1045 alterations in secondary metabolism are critical for the uptake of insoluble iron compounds
1046 by Arabidopsis and *Medicago truncatula*. *Plant Physiol* **162**: 1473-1485
- 1047 **Rogers EE, Eide DJ, Guerinot ML** (2000) Altered selectivity in an Arabidopsis metal transporter. *Proc
1048 Natl Acad Sci U S A* **97**: 12356-12360

- 1049 **Santi S, Schmidt W** (2009) Dissecting iron deficiency-induced proton extrusion in Arabidopsis roots.
1050 *New Phytol* **183**: 1072-1084
- 1051 **Schmid NB, Giehl RF, Doll S, Mock HP, Strehmel N, Scheel D, Kong X, Hider RC, von Wiren N** (2014)
1052 Feruloyl-CoA 6'-Hydroxylase1-dependent coumarins mediate iron acquisition from alkaline
1053 substrates in Arabidopsis. *Plant Physiol* **164**: 160-172
- 1054 **Shin LJ, Lo JC, Chen GH, Callis J, Fu H, Yeh KC** (2013) IRT1 degradation factor1, a ring E3 ubiquitin
1055 ligase, regulates the degradation of iron-regulated transporter1 in Arabidopsis. *Plant Cell* **25**:
1056 3039-3051
- 1057 **Singh A, Severance S, Kaur N, Wiltsie W, Kosman DJ** (2006) Assembly, activation, and trafficking of
1058 the Fet3p.Ftr1p high affinity iron permease complex in *Saccharomyces cerevisiae*. *J Biol*
1059 *Chem* **281**: 13355-13364
- 1060 **Tan S, Zhang P, Xiao W, Feng B, Chen LY, Li S, Li P, Zhao WZ, Qi XT, Yin LP** (2018) TMD1 domain and
1061 CRAC motif determine the association and disassociation of MxIRT1 with detergent-resistant
1062 membranes. *Traffic* **19**: 122-137
- 1063 **Thomine S, Vert G** (2013) Iron transport in plants: better be safe than sorry. *Curr Opin Plant Biol* **16**:
1064 322-327
- 1065 **Vert G, Briat JF, Curie C** (2001) Arabidopsis IRT2 gene encodes a root-periphery iron transporter.
1066 *Plant Journal* **26**: 181-189
- 1067 **Vert G, Grotz N, Dedaldechamp F, Gaymard F, Guerinot ML, Briat JF, Curie C** (2002) IRT1, an
1068 Arabidopsis transporter essential for iron uptake from the soil and for plant growth. *Plant*
1069 *Cell* **14**: 1223-1233
- 1070 **von der Haar T** (2007) Optimized protein extraction for quantitative proteomics of yeasts. *PLoS One*
1071 **2**: e1078
- 1072 **Walton A, Stes E, Cybulski N, Van Bel M, Inigo S, Durand AN, Timmerman E, Heyman J, Pauwels L,**
1073 **De Veylder L, Goossens A, De Smet I, Coppens F, Goormachtig S, Gevaert K** (2016) It's Time
1074 for Some "Site"-Seeing: Novel Tools to Monitor the Ubiquitin Landscape in Arabidopsis
1075 thaliana. *Plant Cell* **28**: 6-16
- 1076 **Xing S, Wallmeroth N, Berendzen KW, Grefen C** (2016) Techniques for the Analysis of Protein-
1077 Protein Interactions in Vivo. *Plant Physiol* **171**: 727-758
- 1078 **Yamada K, Nagano AJ, Nishina M, Hara-Nishimura I, Nishimura M** (2013) Identification of two novel
1079 endoplasmic reticulum body-specific integral membrane proteins. *Plant Physiol* **161**: 108-120
- 1080 **Yi Y, Guerinot ML** (1996) Genetic evidence that induction of root Fe(III) chelate reductase activity is
1081 necessary for iron uptake under iron deficiency. *Plant J.* **10**: 835-844
- 1082 **Yorimitsu T, Sato K, Takeuchi M** (2014) Molecular mechanisms of Sar/Arf GTPases in vesicular
1083 trafficking in yeast and plants. *Front Plant Sci* **5**: 411
- 1084 **Yuan W, Zhang D, Song T, Xu F, Lin S, Xu W, Li Q, Zhu Y, Liang J, Zhang J** (2017) Arabidopsis plasma
1085 membrane H⁺-ATPase genes *AHA2* and *AHA7* have distinct and overlapping roles in the
1086 modulation of root tip H⁺ efflux in response to low-phosphorus stress. *J Exp Bot* **68**: 1731-
1087 1741
- 1088 **Yuan Y, Wu H, Wang N, Li J, Zhao W, Du J, Wang D, Ling HQ** (2008) FIT interacts with AtbHLH38 and
1089 AtbHLH39 in regulating iron uptake gene expression for iron homeostasis in Arabidopsis. *Cell*
1090 *Res* **18**: 385-397
- 1091 **Zelazny E, Barberon M, Curie C, Vert G** (2011) Ubiquitination of transporters at the forefront of plant
1092 nutrition. *Plant Signal Behav* **6**: 1597-1599
- 1093 **Zelazny E, Borst JW, Muylaert M, Batoko H, Hemminga MA, Chaumont F** (2007) FRET imaging in
1094 living maize cells reveals that plasma membrane aquaporins interact to regulate their
1095 subcellular localization. *Proc Natl Acad Sci U S A* **104**: 12359-12364
- 1096 **Zelazny E, Miecielica U, Borst JW, Hemminga MA, Chaumont F** (2009) An N-terminal diacidic motif is
1097 required for the trafficking of maize aquaporins ZmPIP2;4 and ZmPIP2;5 to the plasma
1098 membrane. *Plant J* **57**: 346-355
- 1099 **Zhang J, Li W, Xiang T, Liu Z, Laluk K, Ding X, Zou Y, Gao M, Zhang X, Chen S, Mengiste T, Zhang Y,**
1100 **Zhou JM** (2010) Receptor-like cytoplasmic kinases integrate signaling from multiple plant

1101 immune receptors and are targeted by a *Pseudomonas syringae* effector. *Cell Host Microbe*
1102 **7**: 290-301
1103

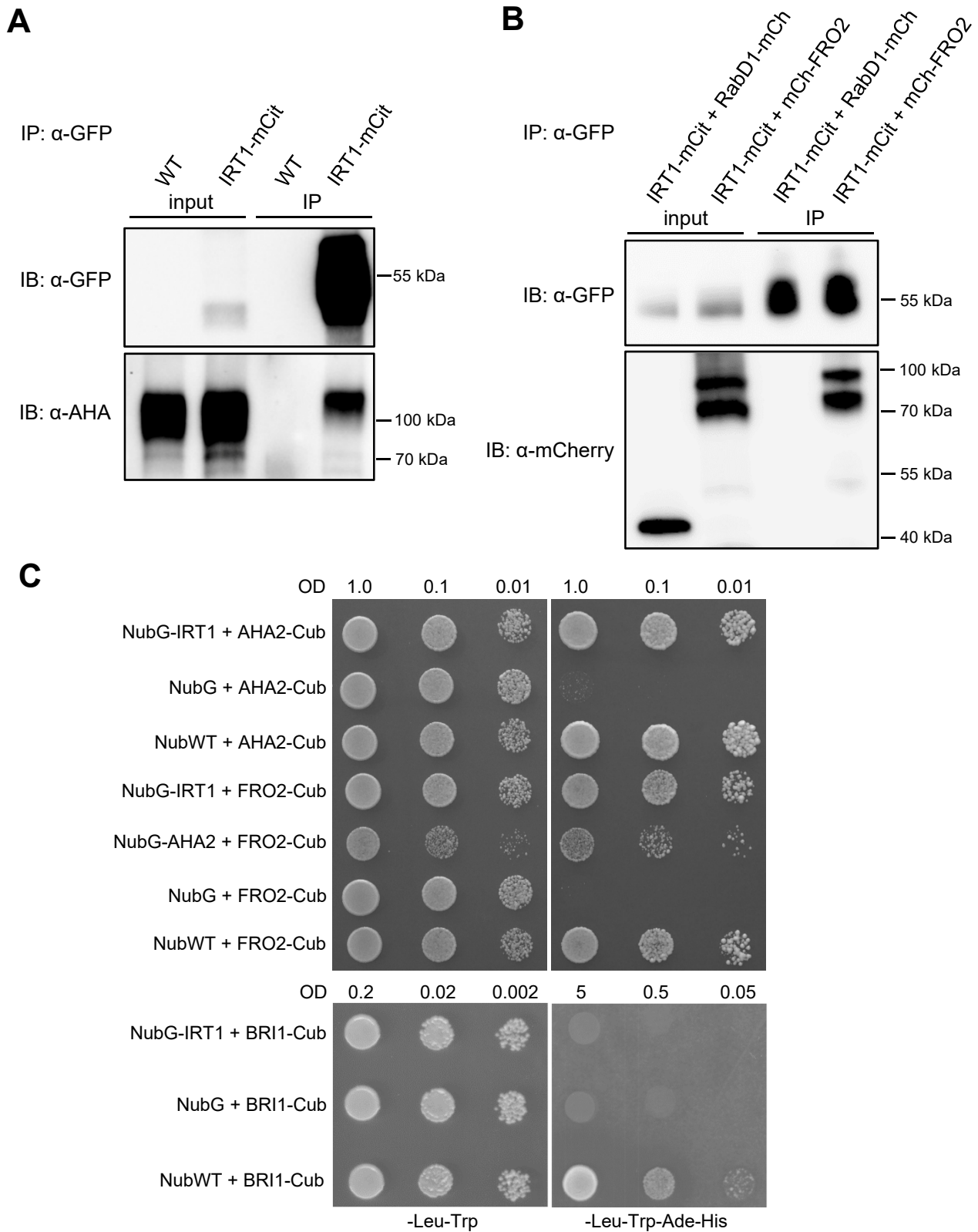


Figure 1. FRO2 and AHA2 are part of an IRT1-protein complex.

(A) Endogenous AHA2 is co-immunopurified with IRT1-mCitrine in *Arabidopsis* root cells. Immunopurifications (IP) were performed using anti-GFP antibodies on solubilized root protein extracts from *irt1-1*/IRT1::IRT1-mCitrine and wild-type plants (negative control). Inputs and IP fractions were subjected to immunoblotting (IB) with anti-GFP (top) and anti-AHA/PMA2 antibodies (bottom).

Figure 1. (continued)

(B) mCherry-FRO2 is co-immunopurified with IRT1-mCitrine in *Arabidopsis* root cells. IP were performed using anti-GFP antibodies on solubilized root protein extracts from *irt1-1/IRT1::IRT1-mCitrine* plants co-expressing FRO2::mCherry-FRO2 or UBQ10::RabD1-mCherry, this protein co-localizing with IRT1 in endosomes (negative control). Inputs and IP fractions were subjected to IB with anti-GFP (top) and anti-mCherry antibodies (bottom). Note that mCherry-FRO2 migrates at the expected size (top band) but also at a lower molecular weight (bottom band). For the co-IP experiments in (A) and (B), roots were harvested from plants grown for 11 days on MS/2 medium containing 50 μ M Fe-EDTA, and then transferred for 4 days on MS/2 medium lacking iron and supplemented with 300 μ M of the iron chelator Ferrozine, in the presence of physiologically relevant concentrations of non-iron metal substrates. Representative immunoblots are shown.

(C) IRT1 directly interacts with FRO2 and AHA2 in a split-ubiquitin assay. Yeasts co-expressing Cub-PLV fusion proteins with NubG fusion proteins or NubG (negative control of interaction) or NubWT (positive control of interaction) were dropped in serial dilutions on a synthetic medium without Leu and Trp (control medium) or without Leu, Trp, His, Ade (selective medium). For the interaction tests between IRT1, FRO2, and AHA2, yeast growth on control and selective media was recorded after 24h and 48h, respectively. Besides internal negative interaction tests performed by co-expressing Cub fusion proteins with NubG, an additional negative control was introduced in this assay by co-expressing NubG-IRT1 and BRI1-Cub. For this IRT1-BRI1 interaction test, yeast growth on control and selective media was recorded after 48h and 72h, respectively. OD: optical density. A representative assay is shown.

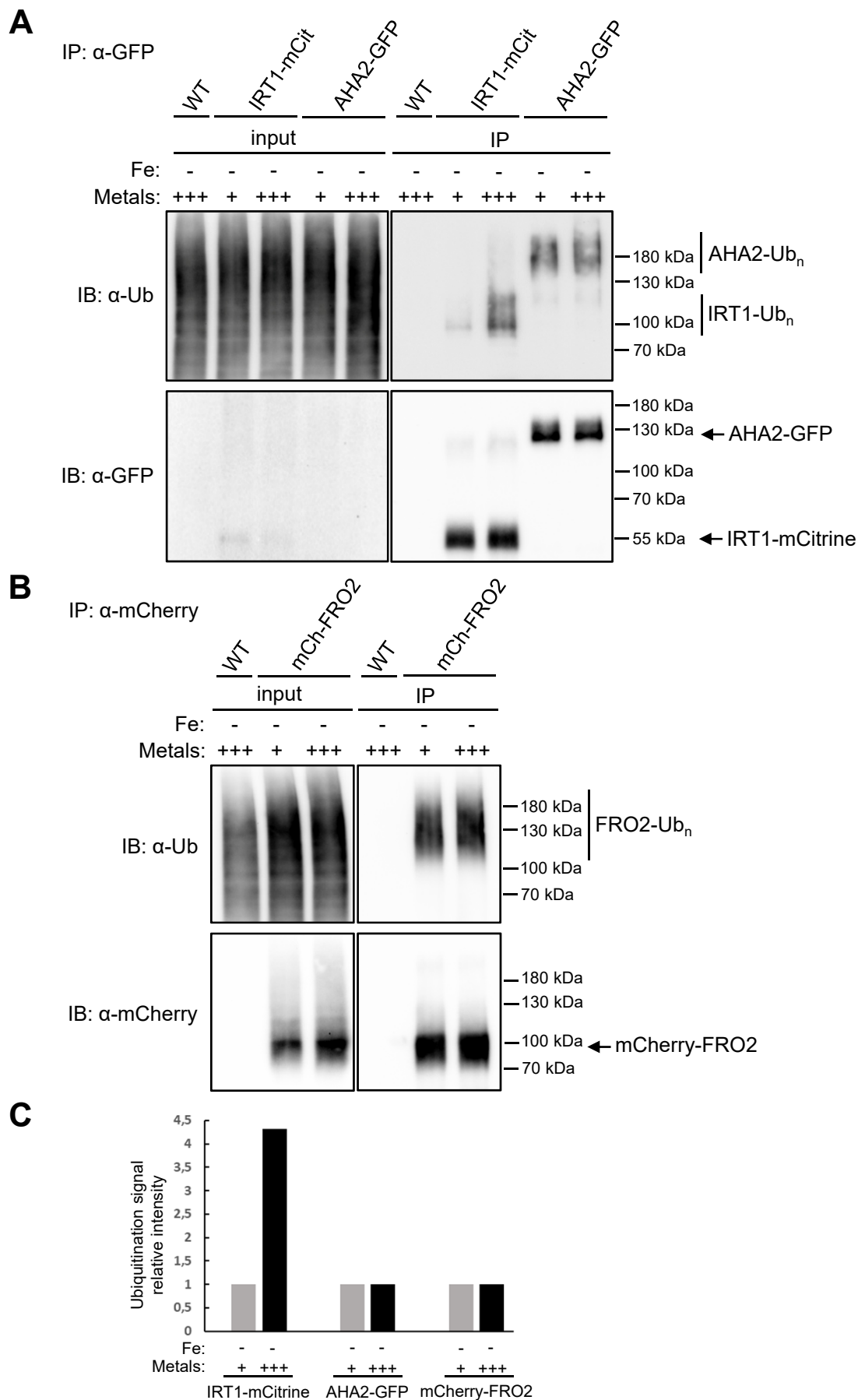


Figure 2. FRO2 and AHA2 are ubiquitinated in *Arabidopsis* root cells in a metal-independent manner.

Immunopurifications (IP) were performed using anti-GFP antibodies on solubilized root protein extracts from wild-type, *irt1-1*/IRT1::IRT1-mCitrine and Col0/35S::AHA2-GFP plants (A) or using anti-mCherry antibodies on solubilized root protein extracts from wild-type and *frd1*/FRO2::mCherry-FRO2 plants (B).

Figure 2 (continued).

Inputs and IP fractions were subjected to immunoblotting (IB) with anti-Ub antibody (P4D1) (A and B, top), anti-GFP (A, bottom), or anti-mCherry antibodies (B, bottom). Non-ubiquitinated and ubiquitinated forms of the studied proteins are indicated by an arrow and a bar ($-Ub_n$), respectively. Roots were harvested from plants grown for 11 days on MS/2 medium lacking iron (-), in the presence of physiologically relevant concentrations of non-iron metal substrates (+), and then transferred for 2 hours to the same medium (control) or to a medium lacking iron and containing an excess of non-iron metals (+++). Wild-type plants were used as negative controls for IP. In (A), due to very low expression level, AHA2-GFP is not detected in inputs but solely in IP fractions after enrichment. (C) Quantification of IRT1-mCitrine, AHA2-GFP, and mCherry-FRO2 ubiquitination in the presence of physiologically relevant concentrations of non-iron metal substrates (+) or an excess of these metals (+++). The intensity of the ubiquitin signal from IRT1-mCitrine, AHA2-GFP, and mCherry-FRO2 IP shown in (A) and (B) was measured using Image Lab and normalized to the quantity of immunopurified proteins. Results are shown as ratio relative to the (+) condition for each protein to reveal the influence of metal treatment.

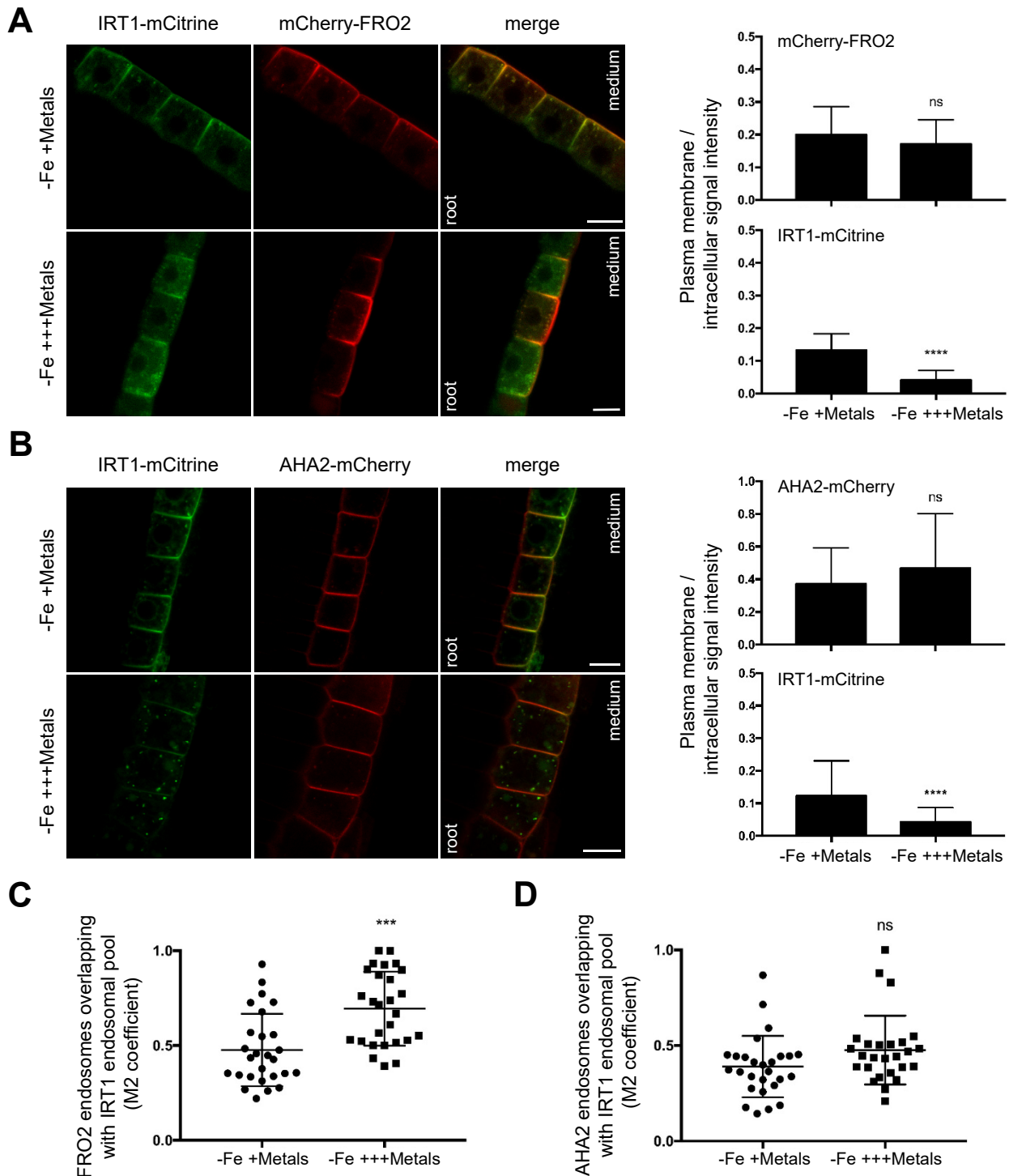


Figure 3. The endocytosis of IRT1 and FRO2/AHA2 is differentially regulated by non-iron metal substrates in root tip epidermal cells.

Confocal microscopy analyses of root epidermal cells from *irt1-1/IRT1::IRT1-mCitrine* plants co-expressing IRT1::mCherry-FRO2 (A, left panel) or IRT1::AHA2-mCherry (B, left panel). Plants were grown for 11 days on MS/2 medium lacking iron, in the presence of physiologically relevant concentrations of non-iron metal substrates, and then transferred for 2 hours to the same medium (-Fe +Metals, control) or to a medium lacking iron and containing an excess of non-iron metals (-Fe +++Metals). To standardize microscopy analysis at the root tip, the same cells located just above the lateral root cap were systematically analyzed. Scale bars, 10 μ m. Representative images are shown. Right panels in (A) and (B) show the ratio of plasma membrane to intracellular signal intensities for IRT1-mCitrine, mCherry-FRO2, and AHA2-mCherry from experiments performed as in the left panels of (A) and (B). Mander's coefficients (M2) of mCherry-FRO2 (C) and AHA2-mCherry (D) endosomal structures showing overlap with IRT1-mCitrine labeled endosomes were calculated from experiments performed as in (A) and (B), left panels. All the quantifications shown in this figure were carried out in triplicates on stacks encompassing epidermal cells. In total, 27 cells were analyzed for each condition and genotype. Error bars represent SD ($n = 27$) for each genotype. The asterisks indicate significant differences to -Fe +Metals (unpaired t-test, $p < 0.0001$).

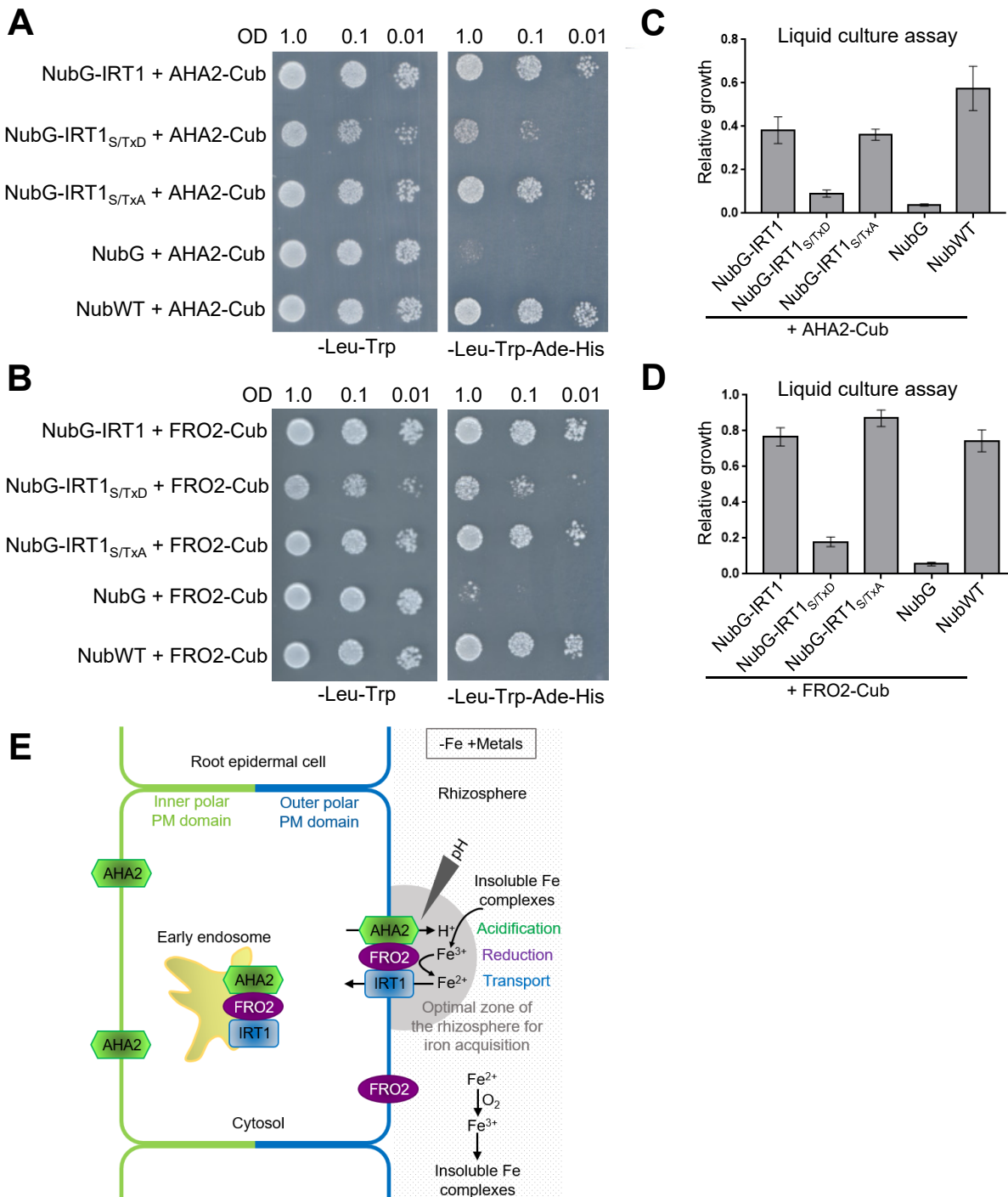


Figure 4. Phosphorylation of IRT1 decreases its interaction with AHA2 and FRO2. Tentative model for the functioning of the iron-acquisition complex.

(A-D) Effect of IRT1 phospho-status on its interaction with AHA2 and FRO2. Split-ubiquitin interaction tests were performed between wild-type IRT1, IRT1 variants for phosphorylation sites (phosphomimic S/TxD and non-phosphorylatable S/TxA) and AHA2 (A), or FRO2 (B). Yeasts were dropped in serial dilutions on a synthetic medium without Leu and Trp (control medium) or without Leu, Trp, His, Ade (selective medium). NubG and NubWT were used as negative and positive controls of interaction, respectively. Yeast growth on control and selective medium was monitored after 48h and 72h, respectively. O.D: optical density. Representative assays are shown. To quantify interactions, the same tests were performed in liquid cultures as shown in (C) and (D). The O.D measured for transformed yeast grown in the selective medium for 24h was normalized to the O.D measured for the same yeast grown in the control medium for 16h (relative growth). Error bars represent SEM, n = 8 in (C) and n = 12 in (D).

Figure 4 (continued)

(E) Putative functioning of the iron-acquisition complex. IRT1, FRO2 and AHA2 proteins interact at the outer polar plasma membrane (PM) domain of root epidermal cells to form a specialized complex that likely optimizes iron acquisition by creating a local environment with low pH and high Fe^{2+} concentration. Outside this optimal zone for iron acquisition, we propose that Fe^{2+} is constantly re-oxidized to Fe^{3+} , which in turn forms insoluble iron complexes. In addition to be plasma membrane localized, the iron-acquisition complex is also probably present in early endosomes, reflecting endocytic events of the complex. Note that contrary to IRT1 and FRO2, AHA2 is distributed at both plasma membrane polar domains. FRO2 might be not exclusively associated with IRT1. This model depicts the localization of IRT1, FRO2, and AHA2 in the absence of iron and in the presence of physiologically relevant concentrations of non-iron metal substrates (-Fe +Metals). Although IRT1, FRO2, and AHA2 interact all together, this feature is not represented to simplify the scheme.

Parsed Citations

Barberon M, Dubeaux G, Kolb C, Isono E, Zelazny E, Vert G (2014) Polarization of IRON-REGULATED TRANSPORTER 1 (IRT1) to the plant-soil interface plays crucial role in metal homeostasis. *Proc Natl Acad Sci U S A* 111: 8293-8298

Google Scholar: [Author Only](#) [Title Only](#) [Author and Title](#)

Barberon M, Zelazny E, Robert S, Conejero G, Curie C, Friml J, Vert G (2011) Monoubiquitin-dependent endocytosis of the iron-regulated transporter 1 (IRT1) transporter controls iron uptake in plants. *Proc Natl Acad Sci U S A* 108: E450-458

Google Scholar: [Author Only](#) [Title Only](#) [Author and Title](#)

Bellati J, Champeyroux C, Hem S, Rofidal V, Krouk G, Maurel C, Santoni V (2016) Novel Aquaporin Regulatory Mechanisms Revealed by Interactomics. *Mol Cell Proteomics* 15: 3473-3487

Google Scholar: [Author Only](#) [Title Only](#) [Author and Title](#)

Blanchet S, Cornu D, Argentini M, Namy O (2014) New insights into the incorporation of natural suppressor tRNAs at stop codons in *Saccharomyces cerevisiae*. *Nucleic Acids Res* 42: 10061-10072

Google Scholar: [Author Only](#) [Title Only](#) [Author and Title](#)

Briat JF, Dubos C, Gaymard F (2015) Iron nutrition, biomass production, and plant product quality. *Trends Plant Sci* 20: 33-40

Google Scholar: [Author Only](#) [Title Only](#) [Author and Title](#)

Chung KP, Zeng Y, Jiang L (2016) COPII Paralogs in Plants: Functional Redundancy or Diversity? *Trends Plant Sci* 21: 758-769

Google Scholar: [Author Only](#) [Title Only](#) [Author and Title](#)

Cointry V, Vert G (2019) The bifunctional transporter-receptor IRT1 at the heart of metal sensing and signalling. *New Phytol* 223: 1173-1178

Google Scholar: [Author Only](#) [Title Only](#) [Author and Title](#)

Colangelo EP, Guerinot ML (2004) The essential basic helix-loop-helix protein FIT1 is required for the iron deficiency response. *Plant Cell* 16: 3400-3412

Google Scholar: [Author Only](#) [Title Only](#) [Author and Title](#)

Connolly EL, Campbell NH, Grotz N, Prichard CL, Guerinot ML (2003) Overexpression of the FRO2 ferric chelate reductase confers tolerance to growth on low iron and uncovers posttranscriptional control. *Plant Physiol* 133: 1102-1110

Google Scholar: [Author Only](#) [Title Only](#) [Author and Title](#)

Couto D, Niebergall R, Liang X, Bucherl CA, Sklenar J, Macho AP, Ntoukakis V, Derbyshire P, Altenbach D, Maclean D, Robotzek S, Uhrig J, Menke F, Zhou JM, Zipfel C (2016) The Arabidopsis Protein Phosphatase PP2C38 Negatively Regulates the Central Immune Kinase BIK1. *PLoS Pathog* 12: e1005811

Google Scholar: [Author Only](#) [Title Only](#) [Author and Title](#)

Dettmer J, Hong-Hermesdorf A, Stierhof YD, Schumacher K (2006) Vacuolar H⁺-ATPase activity is required for endocytic and secretory trafficking in Arabidopsis. *Plant Cell* 18: 715-730

Google Scholar: [Author Only](#) [Title Only](#) [Author and Title](#)

Dubeaux G, Neveu J, Zelazny E, Vert G (2018) Metal Sensing by the IRT1 Transporter-Receptor Orchestrates Its Own Degradation and Plant Metal Nutrition. *Mol Cell* 69: 953-964 e955

Google Scholar: [Author Only](#) [Title Only](#) [Author and Title](#)

Eide D, Broderius M, Fett J, Guerinot ML (1996) A novel iron-regulated metal transporter from plants identified by functional expression in yeast. *Proceedings of the National Academy of Sciences of the United States of America* 93: 5624-5628

Google Scholar: [Author Only](#) [Title Only](#) [Author and Title](#)

Fan L, Li R, Pan J, Ding Z, Lin J (2015) Endocytosis and its regulation in plants. *Trends Plant Sci* 20: 388-397

Google Scholar: [Author Only](#) [Title Only](#) [Author and Title](#)

Fourcroy P, Siso-Terraza P, Sudre D, Saviron M, Reyt G, Gaymard F, Abadia A, Abadia J, Alvarez-Fernandez A, Briat JF (2014) Involvement of the ABCG37 transporter in secretion of scopoletin and derivatives by Arabidopsis roots in response to iron deficiency. *New Phytol* 201: 155-167

Google Scholar: [Author Only](#) [Title Only](#) [Author and Title](#)

Fourcroy P, Tissot N, Gaymard F, Briat JF, Dubos C (2016) Facilitated Fe Nutrition by Phenolic Compounds Excreted by the Arabidopsis ABCG37/PDR9 Transporter Requires the IRT1/FRO2 High-Affinity Root Fe(2+) Transport System. *Mol Plant* 9: 485-488

Google Scholar: [Author Only](#) [Title Only](#) [Author and Title](#)

Gao C, Luo M, Zhao Q, Yang R, Cui Y, Zeng Y, Xia J, Jiang L (2014) A unique plant ESCRT component, FREE1, regulates multivesicular body protein sorting and plant growth. *Curr Biol* 24: 2556-2563

Google Scholar: [Author Only](#) [Title Only](#) [Author and Title](#)

Geldner N, Denervaud-Tendon V, Hyman DL, Mayer U, Stierhof YD, Chory J (2009) Rapid, combinatorial analysis of membrane

compartments in intact plants with a multicolor marker set. *Plant J* 59: 169-178

Google Scholar: [Author Only](#) [Title Only](#) [Author and Title](#)

Hachez C, Laloux T, Reinhardt H, Cavez D, Degand H, Grefen C, De Rycke R, Inze D, Blatt MR, Russinova E, Chaumont F (2014) *Arabidopsis* SNAREs SYP61 and SYP121 coordinate the trafficking of plasma membrane aquaporin PIP2;7 to modulate the cell membrane water permeability. *Plant Cell* 26: 3132-3147

Google Scholar: [Author Only](#) [Title Only](#) [Author and Title](#)

Haruta M, Tan LX, Bushey DB, Swanson SJ, Sussman MR (2018) Environmental and Genetic Factors Regulating Localization of the Plant Plasma Membrane H(+)-ATPase. *Plant Physiol* 176: 364-377

Google Scholar: [Author Only](#) [Title Only](#) [Author and Title](#)

Hoffmann RD, Olsen LI, Ezike CV, Pedersen JT, Manstretta R, Lopez-Marques RL, Palmgren M (2018) Roles of plasma membrane proton ATPases AHA2 and AHA7 in normal growth of roots and root hairs in *Arabidopsis thaliana*. *Physiol Plant*

Google Scholar: [Author Only](#) [Title Only](#) [Author and Title](#)

Inoue H, Kobayashi T, Nozoye T, Takahashi M, Kakei Y, Suzuki K, Nakazono M, Nakanishi H, Mori S, Nishizawa NK (2009) Rice OsYSL15 is an iron-regulated iron(III)-deoxymugineic acid transporter expressed in the roots and is essential for iron uptake in early growth of the seedlings. *J Biol Chem* 284: 3470-3479

Google Scholar: [Author Only](#) [Title Only](#) [Author and Title](#)

Ishimaru Y, Kim S, Tsukamoto T, Oki H, Kobayashi T, Watanabe S, Matsushashi S, Takahashi M, Nakanishi H, Mori S, Nishizawa NK (2007) Mutational reconstructed ferric chelate reductase confers enhanced tolerance in rice to iron deficiency in calcareous soil. *Proc Natl Acad Sci U S A* 104: 7373-7378

Google Scholar: [Author Only](#) [Title Only](#) [Author and Title](#)

Ishimaru Y, Suzuki M, Tsukamoto T, Suzuki K, Nakazono M, Kobayashi T, Wada Y, Watanabe S, Matsushashi S, Takahashi M, Nakanishi H, Mori S, Nishizawa NK (2006) Rice plants take up iron as an Fe³⁺-phytosiderophore and as Fe²⁺. *Plant J* 45: 335-346

Google Scholar: [Author Only](#) [Title Only](#) [Author and Title](#)

Ivanov R, Brumbarova T, Blum A, Jantke AM, Fink-Straube C, Bauer P (2014) SORTING NEXIN1 Is Required for Modulating the Trafficking and Stability of the *Arabidopsis* IRON-REGULATED TRANSPORTER1. *Plant Cell* 26: 1294-1307

Google Scholar: [Author Only](#) [Title Only](#) [Author and Title](#)

Jakoby M, Wang HY, Reidt W, Weisshaar B, Bauer P (2004) FRU (BHLH029) is required for induction of iron mobilization genes in *Arabidopsis thaliana*. *FEBS Lett* 577: 528-534

Google Scholar: [Author Only](#) [Title Only](#) [Author and Title](#)

Jeong J, Merkovich A, Clyne M, Connolly EL (2017) Directing iron transport in dicots: regulation of iron acquisition and translocation. *Curr Opin Plant Biol* 39: 106-113

Google Scholar: [Author Only](#) [Title Only](#) [Author and Title](#)

Johnson A, Vert G (2016) Unraveling K63 Polyubiquitination Networks by Sensor-Based Proteomics. *Plant Physiol* 171: 1808-1820

Google Scholar: [Author Only](#) [Title Only](#) [Author and Title](#)

Karlova R, Boeren S, Russinova E, Aker J, Vervoort J, de Vries S (2006) The *Arabidopsis* SOMATIC EMBRYOGENESIS RECEPTOR-LIKE KINASE1 protein complex includes BRASSINOSTEROID-INSENSITIVE1. *Plant Cell* 18: 626-638

Google Scholar: [Author Only](#) [Title Only](#) [Author and Title](#)

Khan I, Gratz R, Denezhkin P, Schott-Verdugo SN, Angrand K, Genders L, Basgaran RM, Fink-Straube C, Brumbarova T, Gohlke H, Bauer P, Ivanov R (2019) Calcium-promoted interaction between the C2-domain protein EHB1 and metal transporter IRT1 inhibits *Arabidopsis* iron acquisition. *Plant Physiol*

Google Scholar: [Author Only](#) [Title Only](#) [Author and Title](#)

Kim DY, Bove L, Maeshima M, Martinoia E, Lee Y (2007) The ABC transporter AtPDR8 is a cadmium extrusion pump conferring heavy metal resistance. *Plant J* 50: 207-218

Google Scholar: [Author Only](#) [Title Only](#) [Author and Title](#)

Kim DY, Scalf M, Smith LM, Vierstra RD (2013) Advanced proteomic analyses yield a deep catalog of ubiquitylation targets in *Arabidopsis*. *Plant Cell* 25: 1523-1540

Google Scholar: [Author Only](#) [Title Only](#) [Author and Title](#)

Komander D (2009) The emerging complexity of protein ubiquitination. *Biochem Soc Trans* 37: 937-953

Google Scholar: [Author Only](#) [Title Only](#) [Author and Title](#)

Kwok EY, Severance S, Kosman DJ (2006) Evidence for iron channeling in the Fet3p-Ftr1p high-affinity iron uptake complex in the yeast plasma membrane. *Biochemistry* 45: 6317-6327

Google Scholar: [Author Only](#) [Title Only](#) [Author and Title](#)

Lauwers E, Erpapazoglou Z, Haguenaer-Tsapis R, Andre B (2010) The ubiquitin code of yeast permease trafficking. *Trends Cell*

Biol 20: 196-204

Google Scholar: [Author Only](#) [Title Only](#) [Author and Title](#)

Lee S, Chiecko JC, Kim SA, Walker EL, Lee Y, Guerinot ML, An G (2009) Disruption of OsYSL15 leads to iron inefficiency in rice plants. Plant Physiol 150: 786-800

Google Scholar: [Author Only](#) [Title Only](#) [Author and Title](#)

Marques-Bueno MDM, Morao AK, Cayrel A, Platre MP, Barberon M, Caillieux E, Colot V, Jaillais Y, Roudier F, Vert G (2016) A versatile Multisite Gateway-compatible promoter and transgenic line collection for cell type-specific functional genomics in Arabidopsis. Plant J 85: 320-333

Google Scholar: [Author Only](#) [Title Only](#) [Author and Title](#)

Martins S, Dohmann EM, Cayrel A, Johnson A, Fischer W, Pojer F, Satiat-Jeunemaitre B, Jaillais Y, Chory J, Geldner N, Vert G (2015) Internalization and vacuolar targeting of the brassinosteroid hormone receptor BRI1 are regulated by ubiquitination. Nat Commun 6: 6151

Google Scholar: [Author Only](#) [Title Only](#) [Author and Title](#)

Masalkar P, Wallace IS, Hwang JH, Roberts DM (2010) Interaction of cytosolic glutamine synthetase of soybean root nodules with the C-terminal domain of the symbiosome membrane nodulin 26 aquaglyceroporin. J Biol Chem 285: 23880-23888

Google Scholar: [Author Only](#) [Title Only](#) [Author and Title](#)

Morsomme P, Dambly S, Maudoux O, Boutry M (1998) Single point mutations distributed in 10 soluble and membrane regions of the Nicotiana plumbaginifolia plasma membrane PMA2 H⁺-ATPase activate the enzyme and modify the structure of the C-terminal region. J Biol Chem 273: 34837-34842

Google Scholar: [Author Only](#) [Title Only](#) [Author and Title](#)

Olsen RA, Clark RB, Bennett JH (1981) THE ENHANCEMENT OF SOIL FERTILITY BY PLANT-ROOTS. American Scientist 69: 378-384

Google Scholar: [Author Only](#) [Title Only](#) [Author and Title](#)

Pacifici E, Di Mambro R, Dello Iorio R, Costantino P, Sabatini S (2018) Acidic cell elongation drives cell differentiation in the Arabidopsis root. EMBO J 37

Google Scholar: [Author Only](#) [Title Only](#) [Author and Title](#)

Palmer CM, Guerinot ML (2009) Facing the challenges of Cu, Fe and Zn homeostasis in plants. Nat Chem Biol 5: 333-340

Google Scholar: [Author Only](#) [Title Only](#) [Author and Title](#)

Qi X, Zheng H (2013) Rab-A1c GTPase defines a population of the trans-Golgi network that is sensitive to endosidin1 during cytokinesis in Arabidopsis. Mol Plant 6: 847-859

Google Scholar: [Author Only](#) [Title Only](#) [Author and Title](#)

Rajniak J, Giehl RFH, Chang E, Murgia I, von Wiren N, Sattely ES (2018) Biosynthesis of redox-active metabolites in response to iron deficiency in plants. Nat Chem Biol 14: 442-450

Google Scholar: [Author Only](#) [Title Only](#) [Author and Title](#)

Robinson NJ, Procter CM, Connolly EL, Guerinot ML (1999) A ferric-chelate reductase for iron uptake from soils. Nature 397: 694-697

Google Scholar: [Author Only](#) [Title Only](#) [Author and Title](#)

Rodriguez-Celma J, Lin WD, Fu GM, Abadia J, Lopez-Millan AF, Schmidt W (2013) Mutually exclusive alterations in secondary metabolism are critical for the uptake of insoluble iron compounds by Arabidopsis and Medicago truncatula. Plant Physiol 162: 1473-1485

Google Scholar: [Author Only](#) [Title Only](#) [Author and Title](#)

Rogers EE, Eide DJ, Guerinot ML (2000) Altered selectivity in an Arabidopsis metal transporter. Proc Natl Acad Sci U S A 97: 12356-12360

Google Scholar: [Author Only](#) [Title Only](#) [Author and Title](#)

Santi S, Schmidt W (2009) Dissecting iron deficiency-induced proton extrusion in Arabidopsis roots. New Phytol 183: 1072-1084

Google Scholar: [Author Only](#) [Title Only](#) [Author and Title](#)

Schmid NB, Giehl RF, Doll S, Mock HP, Strehmel N, Scheel D, Kong X, Hider RC, von Wiren N (2014) Feruloyl-CoA 6'-Hydroxylase1-dependent coumarins mediate iron acquisition from alkaline substrates in Arabidopsis. Plant Physiol 164: 160-172

Google Scholar: [Author Only](#) [Title Only](#) [Author and Title](#)

Shin LJ, Lo JC, Chen GH, Callis J, Fu H, Yeh KC (2013) IRT1 degradation factor1, a ring E3 ubiquitin ligase, regulates the degradation of iron-regulated transporter1 in Arabidopsis. Plant Cell 25: 3039-3051

Google Scholar: [Author Only](#) [Title Only](#) [Author and Title](#)

Singh A, Severance S, Kaur N, Wiltsie W, Kosman DJ (2006) Assembly, activation, and trafficking of the Fet3p.Ftr1p high affinity

iron permease complex in *Saccharomyces cerevisiae*. J Biol Chem 281: 13355-13364

Google Scholar: [Author Only](#) [Title Only](#) [Author and Title](#)

Tan S, Zhang P, Xiao W, Feng B, Chen LY, Li S, Li P, Zhao WZ, Qi XT, Yin LP (2018) TMD1 domain and CRAC motif determine the association and disassociation of MxlRT1 with detergent-resistant membranes. Traffic 19: 122-137

Google Scholar: [Author Only](#) [Title Only](#) [Author and Title](#)

Thomine S, Vert G (2013) Iron transport in plants: better be safe than sorry. Curr Opin Plant Biol 16: 322-327

Google Scholar: [Author Only](#) [Title Only](#) [Author and Title](#)

Vert G, Briat JF, Curie C (2001) Arabidopsis IRT2 gene encodes a root-periphery iron transporter. Plant Journal 26: 181-189

Google Scholar: [Author Only](#) [Title Only](#) [Author and Title](#)

Vert G, Grotz N, Dedaldechamp F, Gaymard F, Guerinot ML, Briat JF, Curie C (2002) IRT1, an Arabidopsis transporter essential for iron uptake from the soil and for plant growth. Plant Cell 14: 1223-1233

Google Scholar: [Author Only](#) [Title Only](#) [Author and Title](#)

von der Haar T (2007) Optimized protein extraction for quantitative proteomics of yeasts. PLoS One 2: e1078

Google Scholar: [Author Only](#) [Title Only](#) [Author and Title](#)

Walton A, Stes E, Cybulski N, Van Bel M, Inigo S, Durand AN, Timmerman E, Heyman J, Pauwels L, De Veylder L, Goossens A, De Smet I, Coppens F, Goormachtig S, Gevaert K (2016) It's Time for Some "Site"-Seeing: Novel Tools to Monitor the Ubiquitin Landscape in *Arabidopsis thaliana*. Plant Cell 28: 6-16

Google Scholar: [Author Only](#) [Title Only](#) [Author and Title](#)

Xing S, Wallmeroth N, Berendzen KW, Grefen C (2016) Techniques for the Analysis of Protein-Protein Interactions in Vivo. Plant Physiol 171: 727-758

Google Scholar: [Author Only](#) [Title Only](#) [Author and Title](#)

Yamada K, Nagano AJ, Nishina M, Hara-Nishimura I, Nishimura M (2013) Identification of two novel endoplasmic reticulum body-specific integral membrane proteins. Plant Physiol 161: 108-120

Google Scholar: [Author Only](#) [Title Only](#) [Author and Title](#)

Yi Y, Guerinot ML (1996) Genetic evidence that induction of root Fe(III) chelate reductase activity is necessary for iron uptake under iron deficiency. Plant J. 10: 835-844

Google Scholar: [Author Only](#) [Title Only](#) [Author and Title](#)

Yorimitsu T, Sato K, Takeuchi M (2014) Molecular mechanisms of Sar/Arf GTPases in vesicular trafficking in yeast and plants. Front Plant Sci 5: 411

Google Scholar: [Author Only](#) [Title Only](#) [Author and Title](#)

Yuan W, Zhang D, Song T, Xu F, Lin S, Xu W, Li Q, Zhu Y, Liang J, Zhang J (2017) Arabidopsis plasma membrane H⁺-ATPase genes AHA2 and AHA7 have distinct and overlapping roles in the modulation of root tip H⁺ efflux in response to low-phosphorus stress. J Exp Bot 68: 1731-1741

Google Scholar: [Author Only](#) [Title Only](#) [Author and Title](#)

Yuan Y, Wu H, Wang N, Li J, Zhao W, Du J, Wang D, Ling HQ (2008) FIT interacts with AtbHLH38 and AtbHLH39 in regulating iron uptake gene expression for iron homeostasis in Arabidopsis. Cell Res 18: 385-397

Google Scholar: [Author Only](#) [Title Only](#) [Author and Title](#)

Zelazny E, Barberon M, Curie C, Vert G (2011) Ubiquitination of transporters at the forefront of plant nutrition. Plant Signal Behav 6: 1597-1599

Google Scholar: [Author Only](#) [Title Only](#) [Author and Title](#)

Zelazny E, Borst JW, Muylaert M, Batoko H, Hemminga MA, Chaumont F (2007) FRET imaging in living maize cells reveals that plasma membrane aquaporins interact to regulate their subcellular localization. Proc Natl Acad Sci U S A 104: 12359-12364

Google Scholar: [Author Only](#) [Title Only](#) [Author and Title](#)

Zelazny E, Miecielica U, Borst JW, Hemminga MA, Chaumont F (2009) An N-terminal diacidic motif is required for the trafficking of maize aquaporins ZmPIP2;4 and ZmPIP2;5 to the plasma membrane. Plant J 57: 346-355

Google Scholar: [Author Only](#) [Title Only](#) [Author and Title](#)

Zhang J, Li W, Xiang T, Liu Z, Laluk K, Ding X, Zou Y, Gao M, Zhang X, Chen S, Mengiste T, Zhang Y, Zhou JM (2010) Receptor-like cytoplasmic kinases integrate signaling from multiple plant immune receptors and are targeted by a *Pseudomonas syringae* effector. Cell Host Microbe 7: 290-301

Google Scholar: [Author Only](#) [Title Only](#) [Author and Title](#)